HHS Public Access

Author manuscript

Neuron. Author manuscript; available in PMC 2019 November 21.

Published in final edited form as:

Neuron. 2018 November 21; 100(4): 860–875.e7. doi:10.1016/j.neuron.2018.09.025.

Long-term potentiation requires a rapid burst of dendritic mitochondrial fission during induction

Sai Sachin Divakaruni[1,2,3], **Adam M. Van Dyke**[3], **Ramesh Chandra**[4], **Tara A. LeGates**[3], **Minerva Contreras**[3], **Poorna A. Dharmasri**[2,3], **Henry N. Higgs**[5], **Mary Kay Lobo**[4], **Scott M. Thompson**[3], and **Thomas A. Blanpied**[2,3,6]

[1]Medical Scientist Training Program, University of Maryland School of Medicine, Baltimore, MD, USA [2]Program in Neuroscience, University of Maryland School of Medicine, Baltimore, MD, USA [3]Department of Physiology, University of Maryland School of Medicine, Baltimore, MD, USA [4]Department of Anatomy and Neurobiology, University of Maryland School of Medicine, Baltimore, MD, USA [5]Department of Biochemistry, Geisel School of Medicine at Dartmouth College, Hanover, NH, USA [6]Corresponding author and lead contact, tblanpied@som.umaryland.edu

SUMMARY

Synaptic transmission is bioenergetically demanding, and the diverse processes underlying synaptic plasticity elevate these demands. Therefore, mitochondrial functions including ATP synthesis and Ca^{2+} handling, are likely essential for plasticity. Although axonal mitochondria have been extensively analyzed, LTP is predominantly induced postsynaptically, where mitochondria are understudied. Additionally, though mitochondrial fission is essential for their function, signaling pathways that regulate fission in neurons remain poorly understood. We found that NMDAR-dependent LTP induction prompted a rapid burst of dendritic mitochondrial fission, and elevations of mitochondrial matrix Ca^{2+}. The fission burst was triggered by cytosolic Ca^{2+} elevation, and required CaMKII, actin, and Drp1, as well as dynamin 2. Preventing fission impaired mitochondrial matrix Ca^{2+} elevations, structural LTP in cultured neurons, and electrophysiological LTP in hippocampal slices. These data illustrate a novel pathway whereby synaptic activity controls mitochondrial fission, and show that dynamic control of fission regulates plasticity induction perhaps by modulating mitochondrial Ca^{2+} handling.

AUTHOR CONTRIBUTIONS

S.S.D and T.A.B. conceived and directed the project. H.N.H. provided constructs and contributed to design of fission mechanism experiments. A.M.V.D., T.A.L, and S.M.T. contributed to slice electrophysiology experiment design, and A.M.V.D. and T.A.L. collected electrophysiology data. M.K.L. and R.C. provided constructs and R.C. performed *in vivo* stereotactic injections. M.C. performed spine density analysis, subcloning, and primary culture, and P.A.D provided technical support. S.S.D. performed all imaging experiments, analysis, and composed figures. S.S.D and T.A.B. wrote the manuscript, which all authors reviewed and edited.

DECLARATION OF INTERESTS

The authors declare no competing interests.

Keywords

Mitochondria; fission; LTP; dendrite; spine; Drp1; CaMKII; calcium; plasticity; synapse

INTRODUCTION

Neurons continuously modify their synaptic strength to encode memories and to adapt to experience and the environment. Long-term potentiation (LTP) is a critical cellular mechanism of this adaptation (Nicoll, 2017). NMDA receptor (NMDAR)-dependent LTP is triggered by Ca^{2+} influx into dendritic spines and activation of CaMKII, which amplifies synaptic transmission primarily by increasing the number and conductance of AMPA receptors (AMPARs) (Lisman et al., 2012). This functional enhancement is accompanied by dendritic spine growth, via remodeling of spine actin (Okamoto et al., 2009). Importantly, each of these steps executed within the postsynaptic compartment is likely to elevate the bioenergetic burden on the dendrite (Harris et al., 2012). Mitochondria are the principal regulators of cellular metabolism, and therefore their functions and dynamics may be necessary to respond adequately to this burden.

Mitochondrial functions such as ATP synthesis, Ca^{2+} handling, reactive oxygen species (ROS) generation, and glutamate synthesis, are expected to be particularly important for synaptic transmission and plasticity (Fu et al., 2017; Harris et al., 2012; Todorova and Blokland, 2017). Mitochondrial functions are regulated by mitochondrial Ca^{2+} (Llorente-Folch et al., 2015; Rizzuto et al., 2012) and also by mitochondrial dynamics including fission, fusion, and motility (Mishra and Chan, 2016). In neurons, the roles and regulation of axonal mitochondria in synaptic transmission are well described (Misgeld and Schwarz, 2017; Sheng and Cai, 2012), but the majority of LTP mechanisms occur postsynaptically, where mitochondria are less studied. However, mitochondria do occupy a large portion of the dendritic arbor and are frequently close to spines (Fu et al., 2017).

Furthermore, mitochondrial fission has particularly garnered attention in neurons because it is necessary for development (Waterham et al., 2007; Yoon et al., 2016), and because fission impairments are associated with several neurological and psychiatric diseases (Archer, 2013; Flippo and Strack, 2017). Knocking out the required fission regulator Dynamin-related protein 1 (Drp1) in neurons perturbs mitochondrial function, stunts dendrite growth, compromises synapse formation and maintenance, and impairs synaptic transmission (Ishihara et al., 2009; Li et al., 2004; Oettinghaus et al., 2016; Shields et al., 2015). Further, it was recently reported that an increase in Drp1 in dendrites of D1 medium spiny neurons is associated with reduced mitochondrial length and both cellular and behavioral plasticity during early abstinence after repeated cocaine administration (Chandra et al., 2017). However, whether or how fission in dendrites supports ongoing synaptic transmission and plasticity is still unclear. Intriguingly, silencing neurons with TTX increases the ratio of dendritic mitochondrial fusion to fission, while depolarizing neurons with KCl causes the opposite (Li et al., 2004), suggesting that fission is regulated by activity in neurons.

Mechanistically, mitochondrial fission requires Drp1 to execute the separation of the inner and outer mitochondrial membranes (IMM, OMM). Drp1 is a cytosolic GTPase that binds to

receptors on the OMM (Pagliuso et al., 2017). Stepwise constriction of Drp1 helical rings by GTP hydrolysis promotes the constriction and consolidation of the mitochondrial dual lipid bilayer (Basu et al., 2017; Rosenbloom et al., 2014). Fission also requires actin polymerization mediated by the endoplasmic reticulum (ER)-bound formin INF2 (Ji et al., 2015; Korobova et al., 2013) and the mitochondria-bound protein Spire1c (Manor et al., 2015), both because myosin-dependent actin contraction constricts the OMM (Ji et al., 2015; Korobova et al., 2014) and because actin recruits Drp1 to these sites (Hatch et al., 2016; Ji et al., 2015). Although this molecular cascade has been well described in other cell types, less is known about how mitochondrial fission is accomplished in neurons, particularly in dendrites, or how neuronal activity might modulate these mechanisms. Here we tested the hypothesis that dendritic mitochondrial fission is triggered during LTP induction, and is necessary for LTP expression.

RESULTS

Chemical LTP induction increases dendritic mitochondrial fission

Cultured hippocampal neurons transfected with mitochondrial matrix-targeted DsRed (MitoDsRed) and GFP contained densely-packed mitochondria in the soma, scarce and small mitochondria in axons, and tubular mitochondria throughout the dendritic arbor (Fig. 1A). At rest, mitochondria occupied ~62% of dendrite length (0.624 ± 0.063) and rarely moved, and were found at the base of ~88% of dendritic spines (0.876 ± 0.028). Total mitochondrial length scaled linearly with total dendrite length (Fig. 1B, n = 11 cells/7 coverslips/4 cultures, Pearson r = 0.716, p = 0.013; R^2 = 0.513, p < 0.0001). These data suggest that mitochondria are found throughout dendrites and near most synapses, consistent with recent reports (Faits et al., 2016; Fu et al., 2017).

We then refined an established protocol to chemically induced NMDAR-dependent LTP (cLTP) (Araki et al., 2015) in neurons transfected with membrane-targeted mCherry (mem-mCherry) to delineate cell morphology, and super-ecliptic pHluorin (SEP)-tagged GluA1 and GluA2 (SEP-AMPARs) to depict cell-surface AMPARs (Fig. 1C). cLTP stimulation, compared to stimulation in the presence of the competitive NMDAR antagonist APV (+APV), increased dendritic spine volume by ~30% (Fig. 1D, n_{cLTP} = 239 spines/4 cells/2 coverslips/2 cultures, n_{+APV} = 67/3/2/2, $p_{interaction}$ < 0.0001) and surface AMPARs by ~10% (Fig. 1E, $p_{interaction}$ = 0.001), hereby referred to as structural LTP (sLTP).

We found that, cLTP stimulation produced a rapid and transient increase in dendritic mitochondrial fission (Fig. 1F-G, 0.035 ± 0.009 events/μm, n = 7 cells/5 coverslips/2 cultures), hereby referred to as the cLTP fission burst. The fission burst was prevented by APV (Fig. 1F-G, 0.007 ± 0.004 events/μm, n = 7/5/2, $p_{interaction}$ = 0.03, p_{stim}, p_{time}, and $p_{2.5}$ < 0.0001), and temporally preceded structural LTP (sLTP) (Fig. 1D-G, S1A). We subtracted the number of fission events after stimulation by each cell's own baseline, hereby referred to as fission change, to control for any differences between baseline levels of fission between groups. The fission change was ~9-fold greater in cLTP-stimulated cells (Fig. 1H, 0.027 ± 0.006 Δ fission events/μm), than controls (0.003 ± 0.002 Δ fission events/μm, p < 0.001), further indicating that the cLTP fission burst is NMDAR-dependent.

To determine how long mitochondria remained divided, we extended imaging for an extra hour (Fig. S1B). Most of the fission events during the cLTP fission burst (Fig. S1C, $cLTP_{-2.5}$: 0.004 ± 0.002 events/μm, $cLTP_{7.5}$: 0.011 ± 0.002, n = 10 cells/5 coverslips/3 cultures, $p < 0.005$) were sustained even at 112.5 minutes after stimulation (i.e. 97.5 minutes after wash-out) (Fig. S1D, $sustained_{112.5}$: 71.7 ± 9.4%, $re\text{-}fused_{112.5}$: 28.3 ± 8.9%, $p_{112.5} < 0.01$), and the fission event re-fusion rate was consistently low throughout the experiment (Fig. S1C, $p_{refusion} > 0.2$).

Because nearly every spine has a mitochondrion at the base of its neck, we asked whether fission was spatially restricted to the base of potentiated spines. Nearly all spines undergoing sLTP were on a parent dendrite containing a cLTP-evoked fission event in the same field of view (90.3%, data not shown). The distance between sLTP spines and the nearest site of mitochondrial fission in the same parent dendrite was ~7-8 μm (Fig. S1E, median ± 95% CI: 7.59 ± 2.62, n = 65 spines/6 cells/3 coverslips/2 cultures), but only ~1.5% of these fission events occurred at the base of spines. Taking into consideration these data and the relative timecourses of the fission burst and sLTP, we hypothesized that LTP expression requires an increase in dendritic mitochondrial fission during LTP induction.

Mitochondrial fission burst utilizes mechanisms conserved with other cell types

Mitochondrial fission in non-neuronal cell types canonically requires the GTPase Drp1 (Smirnova et al., 2001) and so we asked whether Drp1 was found at sites of cLTP-evoked dendritic fission events. We transfected neurons with GFP-tagged wild-type Drp1 (GFPDrp1, WT Drp1) and MitoDsRed and found growing puncta of GFPDrp1 at evoked fission sites, which separated after fission (Fig. 2A, S2A), as previously reported in other cells (Ji et al., 2015; Lee et al., 2016). We tested whether preventing Drp1 function would prevent the cLTP fission burst by expressing a knockdown-rescue GFP-tagged, single-amino acid (K38A), GTP-null mutant Drp1 (GFPDrp1DN, DN Drp1) (Fig. 2A), which functions as a dominant negative mutant and prevents fission in other cell types (Merrill et al., 2011; Smirnova et al., 2001). DN Drp1 abolished the cLTP fission burst (Fig. 2B, $cLTP_{2.5}$: 0.010 ± 0.002 events/μm, $+APV_{2.5}$: 0.005 ± 0.002, n_{cLTP} = 8 cells/5 coverslips/4 cultures, n_{+APV} = 10/5/4, $p_{interaction} = 0.691$, $p_{2.5} = 0.679$), whereas WT Drp1 did not ($cLTP_{2.5}$: 0.025 ± 0.008 events/μm, $+APV_{2.5}$: 0.007 ± 0.002, n_{cLTP} = 6/5/4, n_{+APV} = 10/5/4, $p_{interaction} < 0.01$, $p_{2.5} < 0.0001$). Furthermore, DN Drp1 prevented the fission change, while cells expressing WT Drp1 maintained a ~10-fold difference (Fig. 2C, $cLTP_{Drp1}$: 0.021 ± 0.004 Δ events/μm, $+APV_{Drp1}$: 0.002 ± 0.001, $cLTP_{DN}$: 0.007 ± 0.002, $+APV_{DN}$ = 0.0001 ± 0.001, $p_{interaction}$ = 0.006, $p_{Drp1} < 0.0001$, $p_{DN} = 0.1$). Directly comparing the two expression groups further suggested that the burst ($p_{2.5} = 0.0003$) and change from baseline ($p_{cLTP} = 0.0006$) require Drp1 function (Fig. 2B-C).

To ensure that this effect was not due to differential expression levels of Drp1, we performed immunocytochemistry for Drp1 in cells expressing MitoDsRed and GFP, GFPDrp1, or GFPDrp1DN (Fig. S2B). The Drp1 staining intensity in dendrites (GFP: 2091 ± 231.7 AU, GFPDrp1: 2039 ± 335.5, GFPDrp1DN: 1863 ± 200.1) was not significantly different between the three groups (Fig. S2C, n_{GFP} = 15 cells/5 coverslips/2 cultures, n_{Drp1} = 9/4/2, n_{DN} = 12/5/2, $p = 0.334$). Furthermore, neither the cLTP fission burst (Fig. S2D, $cLTP_{GFP}$:

0.034 ± 0.006 events/μm, +APV$_{GFP}$: 0.002 ± 0.002, $p_{interaction}$ = 0.647, $p_{2.5}$ = 0.631) nor the fission change (Fig. S2E, cLTP$_{GFP}$: 0.032 ± 0.006 Δ events/μm, +APV$_{GFP}$: −0.0001 ± 0.001, $p_{interaction}$ = 0.026, $p_{expression}$ = 0.114, p_{cLTP} = 0.095) were significantly different between cells expressing GFP or GFPDrp1 (GFP: n_{cLTP} = 3 cells/2 coverslips/2 cultures, n_{APV} = 7/3/2).

Additionally, to rule out potential off-target effects of expressing DN Drp1 on a knockdown background, we tested the effect of Drp1 knockdown alone by transfecting GFP and Drp1 miRNA (miR) or control miRNA (control) (Fig. S3A), which had previously been used to achieve a somewhat limited 44% knockdown of Drp1 (Chandra et al., 2017). After 4 days, Drp1 miR reduced dendritic Drp1 staining intensity by ~34% compared to controls (Fig. S3B, control: 143.3 ± 19.0 AU, miR: 93.9 ± 7.4, $n_{control}$ = 14 cells/6 coverslips/3 cultures; n_{miR} = 15/5/3, $p < 0.05$). However, we did not observe an effect on the cLTP fission burst (Fig. S3D-E, control: 0.010 ± 0.003 events/μm, miR: 0.006 ± 0.002, $n_{control}$ = 9 cells/4 coverslips/3 cultures, n_{miR} = 11/5/3, $p_{interaction}$ = 0.81) or the fission change after 4 days (Fig. S3F, control: 0.008 ± 0.002 Δ events/μm, miR: 0.005 ± 0.002, p = 0.395). Therefore, we extended the expression time to 10 days, which increased the reduction of Drp1 staining to ~43% (Fig. S3C, control: 99.0 ± 10.07 AU, miR: 56.8 ± 9.0, $n_{control}$ = 16 cells/4 coverslips/2 cultures, n_{miR} = 15/4/2, p = 0.004). Furthermore, 10-day knockdown suppressed both the fission burst (Fig. S3G, control: 0.016 ± 0.002 events/μm, miR: 0.007 ± 0.002, $n_{control}$ = 19 cells/4 coverslips/2 cultures, n_{miR} = 17/3/2, $p_{interaction} < 0.0001$, $p_{2.5} < 0.0001$) and the fission change by ~57% (Fig. 2D, control: 0.014 ± 0.002 Δ events/μm, miR: 0.006 ± 0.001, p = 0.001). These data further support that the cLTP fission burst is Drp1-dependent.

We also tested whether more acutely prohibiting Drp1 function with a pharmacological inhibitor, Mdivi-1 (Cassidy-Stone et al., 2008), would similarly prevent the fission burst. Mdivi-1 (10 μM, 1-2 hr) suppressed both the cLTP fission burst (Fig. S3H, Mdivi-1: 0.015 ± 0.003 events/μm, DMSO: 0.022 ± 0.004, $n_{Mdivi-1}$ = 16 cells/6 coverslips/5 cultures, n_{DMSO} = 21/6/5, $p_{time} < 0.0001$, $p_{2.5}$ = 0.0006) as well as the fission change by ~39% compared to DMSO control (Fig. S3I, Mdivi-1: 0.011 ± 0.002 Δ events/μm, DMSO: 0.018 ± 0.002, p = 0.010). However, Mdivi-1 may have off-target effects in neurons, such as on Complex I of the electron transport chain (Bordt et al., 2017), which may also contribute to its effect on fission. Nevertheless, our data using DN Drp1, Drp1 miR, and Mdivi-1 taken together suggest that the cLTP fission burst requires Drp1.

Because actin polymerization is also required for fission in non-neuronal cells (Hatch et al., 2014), we predicted that perturbing actin dynamics would prevent the cLTP fission burst. We treated cells expressing GFP and MitoDsRed with either Jasplakinolide (500 nM, 1-2 hr), an actin depolymerization inhibitor, or Latrunculin A (10 μM, 1-2 hr), an actin polymerization inhibitor. Both inhibitors impaired the fission burst (Fig. 2E, DMSO: 0.027 ± 0.004 events/μm, Jasp: 0.014 ± 0.003, LatA: 0.016 ± 0.003, n_{DMSO} = 13 cells/5 coverslips/3 cultures, n_{Jasp} = 8/3/3, n_{LatA} = 13/3/3, $p_{interaction}$ = 0.263, $p_{treatment}$ = 0.001, $p_{Jasp} < 0.0001$, $p_{LatA} < 0.0001$) and the fission change by ~50% compared to DMSO controls (Fig. 2F, DMSO: 0.022 ± 0.003 Δ events/μm, Jasp: 0.010 ± 0.003, LatA: 0.011 ± 0.002, p_{ANOVA} = 0.019, p_{Jasp} = 0.047, p_{LatA} = 0.025), suggesting that actin dynamics contribute to the cLTP fission burst.

A recent study found that mitochondrial membrane scission is mediated downstream of Drp1-dependent constriction by Dyn2, a ubiquitously expressed dynamin GTPase (Lee et al., 2016). However, this had yet to be reported in neurons. We tested whether the cLTP fission burst required Dyn2 by expressing MitoDsRed and GFP-tagged wild-type Dyn2 (GFPDyn2, WT Dyn2) or a single amino acid (K44A) GTP-null mutant Dyn2 (GFPDyn2DN, DN Dyn2) (Fig. 2G), which was shown to prevent fission in non-neuronal cells (Lee et al., 2016). Compared to WT Dyn2, DN Dyn2 reduced the cLTP fission burst by ~63% (Fig. 2H, DN: 0.006 ± 0.002 events/μm, Dyn2: 0.016 ± 0.003 events/μm, n_{DN} = 12 cells/5 coverslips/4 cultures, n_{Dyn2} = 12/7/4, $p_{interaction}$ = 0.03, $p_{2.5} < 0.0001$) and the fission change by ~75% (Fig. 2I, DN: 0.003 ± 0.001 Δ events/μm, Dyn2: 0.012 ± 0.002 Δ events/μm, p = 0.0001). These data implicate Dyn2 in neuronal mitochondrial fission for the first time and indicate that the cLTP fission burst requires Dyn2 function, in addition to Drp1 and actin. Taken together, this body of data suggests that the cLTP-evoked dendritic mitochondrial fission burst utilizes mechanisms conserved with other cell types.

Mitochondrial fission selectively occurs at sites of cytosolic calcium elevation

Because the cLTP fission burst was dependent on activation of NMDARs (Fig. 1F-H), which are Ca^{2+}-permeable, we predicted that fission occurs selectively at sites of elevated dendritic Ca^{2+}. To test this, we adapted a glutamate photolysis protocol, which is known to induce LTP via postsynaptic Ca^{2+} influx (Chang et al., 2017; Fu et al., 2017; Sinnen et al., 2017), and targeted several spines along a single parent dendrite in cells expressing GCaMP6f and MitoDsRed (Fig. 3A,E). Dendritic GCaMP6f intensity increased and decayed after each laser pulse and returned to baseline at the end of the train (Fig. 3B), similar to spine GCaMP6f during single-spine photolysis (Chang et al., 2017), and also was restricted to dendritic branches near the sites of glutamate photolysis in every cell imaged (Fig. 3C-D, $\Delta F/F_{unstim}$: −0.139, $\Delta F/F_{stim}$: 0.866, n = 13 cells/8 cs/3 cultures, p < 0.0001). Furthermore, mitochondria within dendritic branches experiencing an increase in GCaMP6f ΔF/F (Fig. 3C-D) underwent ~15-fold more fission events (Fig. 3E-G, 0.044 ± 0.017 events/μm) than in control branches (0.003 ± 0.002 events/μm). This fission increase occurred soon after the stimulation ($p_{interaction}$ = 0.011, $p_{1.5}$ = 0.0003), similar to the cLTP fission burst (Fig. 1G).

We asked whether the change in dendritic Ca^{2+} is a predictor of fission. Because the density of fission events was low and the total dendrite length analyzable in this assay was restricted by the spread of Ca^{2+} elevation following photolysis, which varied cell to cell, we excluded regions that did not have a fission event immediately after stimulation (Fig. 3H, gray circles). In regions that had a fission event after the train (Fig. 3H, blue circles), GCaMP6f ΔF/F and fission events/μm were tightly correlated (Spearman r = 0.655, p = 0.034), and ΔF/F was a significant predictor of fission (R^2 = 0.546, p = 0.009). Thus, our results suggest that NMDAR activation during LTP induction initiates the mitochondrial fission machinery through a Ca^{2+}-dependent mechanism.

CaMKII and Drp1 phosphorylation are required for mitochondrial fission burst

We next asked how cytosolic Ca^{2+} fluctuations are conveyed to the mitochondrial fission machinery. CaMKII is an essential kinase for LTP (Lisman et al., 2012) and was recently suggested to decrease mitochondrial length by phosphorylating Drp1 at serine 616 in

cardiomyocytes (Xu et al., 2016). To test the role of CaMKII, we treated cells expressing GFP and MitoDsRed with the specific inhibitor of CaMKII, KN-93. KN-93 (10 μM, 1-2 hr) abolished the fission burst (Fig. 4A, 93: 0.006 ± 0.002 events/μm, 92: 0.015 ± 0.003, n_{93} = 9 cells/4 coverslips/4 cultures, n_{92} = 13/4/4, p_{drugs} = 0.044, $p_{2.5}$ < 0.005) and the fission change by ~90% (Fig. 4B, 93: 0.001 ± 0.002 Δ events/μm, 92: 0.009 ± 0.002, p = 0.013) compared to the inactive form, KN-92 (10 μM, 1-2 hr), suggesting that the cLTP fission burst requires CaMKII activation. Because the role of CaMKII in regulating neuronal mitochondrial fission is essentially untested, we also asked whether CaMKII is capable of regulating dendritic mitochondrial length at baseline, outside the context of LTP. We expressed GFP, or GFP-tagged wild-type (WT), constitutively active (T286D; CA), or dominant negative (K42M; DN) variants of CaMKII (Fig. S4). WT CaMKII did not affect mitochondrial length compared to cells expressing GFP alone (Fig. 4C, median ± 95% CI - GFP: 1.524 ± 0.181 μm, WT: 1.653 ± 0.005, n_{GFP} = 1241 mitochondria/4 cells/3 coverslips/3 cultures, n_{WT} = 4369/9/5/3, p_{ANOVA} < 0.0001, p_{WT} = 0.174). However, CA CaMKII decreased mitochondrial length (1.188 ± 0.026 μm, n_{CA} = 7910/20/5/3, p_{CA} < 0.0001), and DN CaMKII increased length (1.756 ± 0.077, n_{DN} = 6453/16/5/3, p_{DN} = 0.049), compared to WT CaMKII, suggesting that CaMKII is dynamically involved in regulating neuronal mitochondrial length over a range of activity levels.

We then asked whether Drp1 phosphorylation at Ser616, a possible substrate for CaMKII based on previous studies, was required for the cLTP fission burst. We expressed phospho-null (S616A; inactive) and phospho-mimetic (S616D; active) variants of GFPDrp1, similar to previous reports (Fig. 4D) (Cho et al., 2014). Compared to WT Drp1 (Fig. 4E, Drp1: 0.013 ± 0.002 events/μm, n_{Drp1} = 6 cells/2 coverslips/2 cultures), phospho-null Drp1 suppressed the fission burst by ~69% (S616A: 0.004 ± 0.002, n_{S616A} = 6/3/2, p_{groups} < 0.0001, p_{S616A} = 0.0003), while the S616D mutant enhanced the fission burst by ~54% (S616D: 0.020 ± 0.006, n_{S616DD} = 5/2/2, p_{S616D} = 0.007). Baseline fission rate was ~3.5-fold higher in the S616D neurons (Fig. 4F, S616D: 0.007 ± 0.002 events/μm, p_{ANOVA} = 0.027, p_{S616D} = 0.041), as expected from a hyperactive mutant, but no different in the S616A group (S616A: 0.001 ± 0.001, p_{S616A} = 0.951), compared to neurons expressing WT Drp1 (Drp1: 0.002 ± 0.0005). Lastly, the S616A mutant produced a robust and statistically-trending ~82% reduction in the fission change compared to WT Drp1, consistent with the fission burst data (Fig. 4G, Drp1: 0.011 ± 0.002 Δ events/μm, S616A: 0.002 ± 0.001, S616D: 0.014 ± 0.005, p_{ANOVA} = 0.127). Together, these data suggest that CaMKII activation and Drp1 phosphorylation at Ser616 are required for the cLTP fission burst.

Dendritic mitochondrial fission is required for spine structural LTP

The cLTP fission burst (Fig. 1G) preceded dendritic spine sLTP (Fig. 1D-E), suggesting it may be a prerequisite for LTP expression. We tested this by transfecting cells with mem-mCherry and either GFPDrp1 or GFPDrp1DN (Fig. 5A) and determined that spines in GFPDrp1 cells underwent sLTP (Fig. 5B, n_{cLTP} = 518 spines/10 cells/6 coverslips/5 cultures, n_{+APV} = 133/4/3/3, $p_{interaction}$ < 0.0001). Although spines in DN Drp1 cells also underwent sLTP (Fig. 5B, n_{cLTP} = 267/6/6/6, n_{+APV} = 571/15/8/6, $p_{interaction}$ < 0.0001), the final percent change in spine volume >50 mins after cLTP stimulation was reduced by ~60%, compared to cells expressing WT Drp1 (Fig. 5C, Drp1: 11.050 ± 1.356 %, DN: 4.564

± 1.391, $p_{interaction}$ = 0.056, $p_{expression}$ = 0.008, p_{cLTP} = 0.001). These findings suggest that fission contributes substantially to dendritic spine structural remodeling.

To determine whether fission is required for the amplification of synaptic AMPARs, we immunocytochemically labeled GluA2 and Homer1, a postsynaptic scaffolding protein (Fig. S5A). Among untransfected cells, those that received cLTP stimulation had ~30% greater surface synaptic AMPAR intensity (Fig. 5D, 2907 ± 110.3 AU, n_{cLTP} = 498 synapses/≥17 cells/9 coverslips/3 cultures) than unstimulated cells (2160 ± 85.5, n_{unstim} = 476/≥16/9/3, p_{ANOVA} < 0.0001, p_{unstim} < 0.0001) or +APV-stimulated controls (2362 ± 106, n_{+APV} = 286/≥8/5/3, p_{+APV} = 0.002). Similarly, within the GFPDrp1 group, cLTP-stimulated neurons had ~45% greater AMPAR intensity (Fig. 5E, 2704 ± 157.6, n_{cLTP} = 249/6/3/2) than unstimulated (1878 ± 61.6, n_{unstim} = 546/9/4/2, p_{ANOVA} < 0.0001, p_{unstim} < 0.0001) or +APV-stimulated cells (1771 ± 96, $n+_{APV}$ = 134/2/2/2, p_{+APV} < 0.0001). However, DN Drp1 eliminated the difference in AMPAR staining intensity (Fig. 5F). Within this group, cLTP-stimulated cells did not have greater staining intensity (2394 ± 175.6 AU, n_{cLTP} = 217/11/6/3) than unstimulated (2020 ± 105.7 AU, n_{unstim} = 231/7/5/3, p_{ANOVA} = 0.028, p_{unstim} = 0.129) or +APV-stimulated cells (2537 ± 133, n_{+APV} = 181/6/3/3, p_{+APV} = 0.767), suggesting that mitochondrial fission is required for the increase in surface synaptic AMPARs during LTP.

To assess synaptic AMPARs before and after stimulation within the same spine, we imaged SEP-AMPARs after Drp1 knockdown, which suppressed the cLTP fission burst (Figs. S3G, 2D). Surface AMPAR trafficking (Fig. 5G) was significantly impaired by Drp1 miR compared to controls (Fig. S5K, n_{miR} = 562 spines/13 cells/3 coverslips/2 cultures, $n_{control}$ = 711/9/3/2, $p_{interaction}$ < 0.0001, $p_{expression}$ < 0.0001, p_{time} < 0.0001). Drp1 miR reduced the percent change of SEP-AMPARs immediately after stimulation by ~59% (Fig. 5H, control: 4.353 ± 0.665, miR: 1.781 ± 0.554, p = 0.003), as well as the final percent increase by ~36% (Fig. 5I, control: 11.168 ± 1.024, miR: 7.176 ± 0.957, p = 0.005). We also tested whether Drp1 knockdown would impair spine sLTP by using mem-mRuby (Fig. S5B). Drp1 miR significantly reduced dendritic spine growth to ~57% of controls (Fig. 5J, $cont_{52.5}$: 1.409 ± 0.035, $miR_{52.5}$: 1.175 ± 0.028, $n_{control}$ = 607 spines/9 cells/2 coverslips/2 cultures, n_{miR} = 494 spines/7 cells/2 coverslips/2 cultures, $p_{interaction}$ < 0.0001, $p_{expression}$ < 0.0001, p_{time} <0.0001). Thus, these data confirm the role of Drp1-dependent mitochondrial fission in dendritic spine growth and surface AMPAR trafficking during LTP.

Since we found Dyn2 to be required for the cLTP fission burst, we asked whether its function was similarly required for sLTP. We expressed mem-mCherry and WT or DN Dyn2 (Fig. S5C). DN Dyn2 prevented dendritic spine growth compared to WT Dyn2 (Fig. S5D, n_{DN} = 414 spines/9 cells/5 coverslips/3 cultures, n_{Dyn2} = 331/9/4/3, $p_{interaction}$ < 0.0001, $p_{expression}$ < 0.0001, p_{time} < 0.0001) and also suppressed the final percent change (Fig. S5E, Dyn2: 7.535 ± 1.535, DN: −3.735 ± 2.736, p = 0.0004). It should be noted that these results may not be due to the effect of DN Dyn2 on the cLTP fission burst alone (Fig. 2H-I), since Dyn2 plays numerous roles in membrane trafficking and the same mutant was previously observed to reduce dendritic spine membrane dynamics (Jaskolski et al., 2009) and AMPAR endocytosis (Carroll et al., 1999). Additionally, in the same cells in which acute Mdivi-1 treatment attenuated the cLTP fission burst (Fig. S2F-G), Mdivi-1 also suppressed spine

growth (Fig. S5F, $n_{Mdivi\text{-}1}$ = 724 spines/16 cells/6 coverslips/5 cultures, n_{DMSO} = 963/21/6/5, $p_{interaction}$ = 0.067, p_{drugs} < 0.0001, p_{time} < 0.0001) and the final percent change in spine size by ~59% (Fig. S5G, Mdivi-1: 3.769 ± 1.314, DMSO: 9.258 ± 1.433, p = 0.005), compared to controls. To determine whether our findings were due to gross changes to dendritic spines at baseline, we measured spine density and baseline spine size. Spine density was not different between cells expressing DN Drp1 (Fig. S5H, 3.64 ± 0.22 spines/μm, n = 15 cells/11 coverslips/4 cultures) or WT Drp1 (3.71 ± 0.46 spines/μm, n = 11/7/3, p = 0.887). Furthermore, DN Drp1 barely altered baseline spine area (Fig. S5I-J, ~5% difference, 0.675 ± 0.009 μm^2, n = 838 spines/21 cells/14 coverslips/6 cultures) compared to WT Drp1 (0.712 ± 0.009 μm^2, n = 651/14/9/5, p = 0.016), suggesting that there were no robust alterations to spines at baseline. Taken together, these experiments demonstrate that dendritic mitochondrial fission is required for dendritic spine growth and surface AMPAR trafficking during LTP.

Mitochondrial fission is required for electrophysiological LTP in hippocampal slices

Having determined that mitochondrial fission is necessary for sLTP in culture, we asked whether fission is required for LTP in brain slices. To test whether LTP induction is associated with alteration of mitochondrial morphology, we utilized a transgenic mouse line that expresses MitoEYFP in forebrain neurons driven by a CaMKII promoter (Chandrasekaran et al., 2006), and prepared acute hippocampal slices. We recorded AMPAR-mediated field excitatory postsynaptic potentials (fEPSPs) in hippocampal area CA1 before and after high-frequency stimulation (HFS) of Schaffer collaterals (Fig. 6A). HFS of slices bathed in normal ACSF produced potentiation lasting at least 35 minutes (LTP), which was prevented by APV in the ACSF (+APV) (Fig. 6B, n_{LTP} = 4 slices, n_{+APV} = 4 slices, $p_{interaction}$ < 0.0001, p_{drug} < 0.0001, p_{time} < 0.0001). HFS-dependent elevation of the fEPSP slope amplitude (Fig. 6C, 211.7 ± 20.21%, $p_{interaction}$ < 0.0001, p_{LTP} < 0.0001) was also prevented by APV (Fig. 6C, +APV: 107.4 ± 4.78, p_{+APV} > 0.9999, $p_{LTPvAPV}$ < 0.0001). Recording was halted at 35 minutes, to preserve slice health for imaging, and the slices were fixed and cleared (Susaki et al., 2014). Mitochondrial length in CA1 stratum radiatum (Fig. 6D) of LTP slices were ~10% shorter than in +APV slices (Fig. 6E, LTP_{length}: 1.556 ± 0.029 μm, LTP_{norm} 94.48 ± 2.55%, $+APV_{length}$: 1.679 ± 0.036, $+APV_{norm}$: 105.5 ± 3.25, p = 0.0396). Since decreased mitochondrial length is indicative of increased fission (Chandra et al., 2017; Kim et al., 2016; Xu et al., 2016), this suggests that LTP induction promotes fission in slices.

We next tested whether fission is required for LTP expression in slices. We prepared acute hippocampal slices from WT mice injected with AAV-*Cre*-GFP and AAV-*Cre*-YFPDrp1 into CA1 of one hippocampus and AAV-*Cre*-YFPDrp1DN into the other. Only slices with visible expression in CA1 alone were used for assessing synaptic transmission. We recorded fEPSPs in CA1 before and after HFS (Fig. 6F), which produced LTP lasting at least 60 minutes in both groups (Fig. 6G). However, HFS produced only mild LTP in DN Drp1 slices (144.63 ± 10.7%, $p_{interaction}$ < 0.0001, p_{DN} = 0.029), but robust LTP in WT Drp1 slices (247.7 ± 21.78, p_{Drp1} < 0.0001). Strikingly, DN Drp1 reduced the magnitude of LTP to ~70% of controls (Fig. 6H, $p_{expression}$ < 0.0001).

To determine whether this effect was due to impaired intrinsic electrophysiological properties of CA1 neurons, we performed whole-cell patch clamp recordings (Fig. S6A). We found no difference between WT or DN Drp1 cells in a battery of assays measuring membrane resistance (Fig. S6B, Drp1: 135.2 ± 11.63 MΩ, DN: 148.8 ± 8.47, n_{Drp1} = 7 slices/4 mice, n_{DN} = 10 slices/6 mice, p = 0.476), capacitance (Fig. S6C, Drp1: 69.83 ± 7.76 pF, DN: 58.31 ± 4.71, p = 0.476), resting membrane potential (Fig. S6D, Drp1: −59.06 ± 2.16 mV, DN: −59.36 ± 3.15, p = 0.610), action potential threshold (Fig. S6E-F, Drp1: −48.88 ± 6.87 mV, DN: −45.94 ± 1.25, p = 0.610), input resistance (Fig. S6G, Drp1: 178.2 ± 28.58 MΩ, DN: 243.6 ± 27.17, p = 0.171), or maximum firing rate (Fig. S6H-I, Drp1: 10.5 ± 3.57 Hz, DN: 10 ± 2.02, p = 0.867). To determine whether the effect on LTP was instead due to impaired basal synaptic transmission, we applied a range of stimulation intensities in WT and DN Drp1-infected slices and quantified the AMPAR-component of the postsynaptic responses, which were indistinguishable between the two groups (Fig. S6J). Indeed, there was no difference in the postsynaptic response between the two groups at a stimulation intensity that produced a fiber volley amplitude of ~0.2 mV (Fig. 6I, Drp1: 0.065 ± 0.015 mV/ms, DN: 0.088 ± 0.025, n_{Drp1} = 8 slices/6 animals, n_{DN} = 9/7, p = 0.448). As such, suppressing mitochondrial fission for 2-3 weeks *in vivo* does not impair basal synaptic transmission or intrinsic electrophysiological properties of CA1 neurons. Taken together, these data suggest that postsynaptic mitochondrial fission is required for electrophysiological LTP of CA3-CA1 synapses.

LTP induction increases dendritic mitochondrial calcium transients (mCaTs)

Mitochondria are important Ca^{2+} buffering organelles (Rizzuto et al., 2012), and early evidence suggested that activity of the mitochondrial Ca^{2+} uniporter (MCU) in the hippocampus is enhanced during HFS-LTP (Stanton and Schanne, 1986). Mitochondrial matrix Ca^{2+} serves many functions that could in turn support LTP such as ATP synthesis, ROS generation, or calcium-induced Ca^{2+} release (Llorente-Folch et al., 2015; Rizzuto et al., 2012). Therefore, we asked whether dendritic mitochondrial fission in the context of LTP induction could regulate the ability of mitochondria to buffer Ca^{2+} (Fig. 6J). To determine whether mitochondrial matrix Ca^{2+} is elevated during LTP induction, we transfected neurons with MitoRGECO, a genetically-encoded red fluorescent matrix Ca^{2+} sensor, and GFP (Fig. 7A). Dendritic mitochondria typically had stable matrix Ca^{2+} at baseline but nearly all mitochondria (87.9 ± 0.05%, data not shown) exhibited transient elevations of mitochondrial Ca^{2+}, hereby referred to as mCaTs, following cLTP stimulation (Fig. 7B-C, G, $cLTP_{base}$: 0.004 ± 0.001 Hz, $cLTP_{stim}$: 0.010 ± 0.0005, n_{cLTP} = 247 mitochondria/9 cells/9 coverslips/5 cultures, $p_{interaction}$ = 0.005, p_{cLTP} < 0.0001), which was prevented by APV (Fig. 7D-G, $+APV_{base}$: 0.002 ± 0.001 Hz, $+APV_{stim}$: 0.004 ± 0.001, n_{+APV} = 76/7/7/5, p_{+APV} = 0.742, $p_{cLTPvAPV}$ < 0.0001). When mCaTs did occur even in the presence of APV, the amplitude (Fig. S7A, $\Delta F/F_{cLTP}$: 2.337 ± 0.146, $\Delta F/F_{+APV}$: 2.156 ± 0.162, $p_{interaction}$ = 0.864, $p_{cLTPvAPV}$ = 0.968), duration (Fig. S7A, $cLTP_{stim}$: 21.929 ± 0.766 s, $+APV_{stim}$: 19.78 ± 1.69, $p_{interaction}$ = 0.409, $p_{cLTPvAPV}$ = 0.754), and area under the curve – a proxy for Ca^{2+} influx (Fig. S7A, $cLTP_{stim}$: 32.908 ± 30.832 ((ΔF/F)*s), $+APV_{stim}$: 24.172 ± 3.578, $p_{interaction}$ = 0.964, $p_{cLTPvAPV}$ = 0.999) – were unaffected, suggesting that mCaTs have a characteristic shape. To our knowledge, these data identify for the first time that dendritic mitochondria experience mCaTs during NDMAR-dependent LTP induction.

Dendritic mitochondrial fission is required for cLTP-evoked mCaTs

Although an increase in matrix Ca^{2+} precedes mitochondrial fission (Chakrabarti et al., 2018; Cho et al., 2017), the effect of fission on mitochondrial Ca^{2+} handling remains understudied. We tested whether preventing mitochondrial fission would impact the cLTP-evoked dendritic mCaTs by expressing MitoRGECO and GFP-tagged WT (Fig. 8A-C) or DN Drp1 (Fig. 8D-F). DN Drp1-expressing neurons experienced a cLTP-evoked increase in dendritic mCaT frequency (Fig. 8G, DN_{base}: 0.001 ± 0.0003 Hz, DN_{stim}: 0.007 ± 0.0003, n_{DN} = 271 mitochondria/8 cells/8 coverslips/4 cultures, $p_{interaction} < 0.0001$, $p_{DN} < 0.0001$) as did neurons expressing WT Drp1 (Fig. 8G, $Drp1_{base}$: 0.001 ± 0.0003, $Drp1_{stim}$: 0.012 ± 0.0003, n_{Drp1} = 345/9/9/4, $p_{Drp1} < 0.0001$). Furthermore, the percent mitochondria exhibiting cLTP-evoked mCaTs (94.6 ± 0.02, data not shown) in neurons expressing Drp1 was similar to neurons expressing GFP alone, as was mCaT frequency ($p_{GFPvDrp1} = 0.1045$). However, compared to WT Drp1, DN Drp1 decreased the cLTP-evoked mCaT frequency by ~42% (Fig. 8G, $p_{Drp1vDN} < 0.0001$), amplitude by ~32% ($\Delta F/F_{Drp1}$: 2.193 ± 0.079, $\Delta F/F_{DN}$: 1.494 ± 0.072, $p_{interaction} = 0.42$, $p_{stim} = 0.006$, $p_{Drp1vDN} < 0.0001$), duration by ~27% (Drp1: 25.866 ± 0.625 s, DN: 18.968 ± 0.739, $p_{interaction} = 0.071$, $p_{stim} = 0.0001$, $p_{Drp1vDN} < 0.0001$), and integrated area by ~52% (Drp1: 32.024 ± 1.467 ((ΔF/F)*s), DN: 15.422 ± 0.949, $p_{interaction} = 0.129$, $p_{stim} = 0.004$, $p_{Drp1vDN} < 0.0001$). Taken together, these data suggest that dendritic mitochondrial fission, in addition to being required for structural and electrophysiological LTP, is required for dendritic mitochondrial Ca^{2+} handling during LTP induction.

DISCUSSION

Several mitochondrial functions including ATP synthesis and Ca^{2+} handling are particularly important for synaptic transmission, and the demand for these functions is likely elevated during LTP (Harris et al., 2012). We observed that during LTP induction, dendritic mitochondria underwent a transient ~10-fold increase in the rate of fission events, which was dependent on cytosolic Ca^{2+}, CaMKII, actin, Drp1 phosphorylation and function, and also Dyn2. LTP induction also prompted transient elevations of mitochondrial matrix Ca^{2+} (mCaTs), which were dependent on fission. Furthermore, preventing mitochondrial fission impaired structural and electrophysiological LTP in cultured neurons and acute hippocampal slices, respectively. Thus, a rapid burst of dendritic mitochondrial fission during LTP induction is required for LTP expression (Fig. 8H).

As delineated in a variety of non-neuronal cell types, mitochondrial fission requires Drp1 and actin polymerization downstream of cytosolic Ca^{2+} elevation (Pagliuso et al., 2017), and in this respect, fission in hippocampal dendrites is canonical. In addition, consistent with recent results in COS-7 and HeLa cells (Lee et al., 2016), interfering with Dyn2 blocked the fission burst, thereby implicating Dyn2 in neuronal fission for the first time. Because Dyn2 is the only dynamin required for neuronal development (Ferguson and De Camilli, 2012), and since mitochondrial fission is also required for development (Ishihara et al., 2009; Wakabayashi et al., 2009), it will be important in future studies to determine whether the essential function of Dyn2 during development is in fission, endocytosis, or both. Furthermore, the core mitochondrial fission machinery is complex but widely conserved,

which raises the questions as to how and when fission molecules are recruited and activated in dendrites of different neuronal subtypes, and in which physiological and pathological contexts these may be involved in addition to LTP.

Elevating cytosolic Ca^{2+} via glutamate photolysis was sufficient to trigger fission in the local dendritic area. In a search for the cytosolic messenger responsible for conveying this Ca^{2+} signal to fission proteins, we tested the role of CaMKII, a kinase necessary for LTP (Lisman et al., 2012). CaMKII regulates actin dynamics during LTP (Okamoto et al., 2009), and actin is required for fission (Hatch et al., 2014). Furthermore, CaMKII may promote fission in neurons and cardiomyocytes by increasing Drp1 phosphorylation at Ser616 and its translocation to mitochondria (Godoy et al., 2014; Xu et al., 2016). However, in *C. elegans* neurons, Unc-43 – a homologue of CaMKII – can phosphorylate Drp1 Ser637, as well as other residues, to suppress its function (Jiang et al., 2015), suggesting the need for further investigation. We found that the LTP fission burst required CaMKII activation and phosphorylation of Drp1 Ser616. This suggests that Ca^{2+} influx through NMDARs activates CaMKII, which then activates the mitochondrial fission machinery to cause the fission burst. We also found that at baseline, manipulating CaMKII activity states changes mitochondrial length, strengthening the conclusion that CaMKII is capable of regulating dendritic mitochondrial shape and dynamics. Therefore, our findings not only reveal an unusually acute activation of fission during LTP induction, but also delineate a novel mechanism by which neuronal activity controls mitochondrial fission rate.

Mitochondrial fission is important for synapse formation and maintenance over long periods (Ishihara et al., 2009; Li et al., 2004), but whether postsynaptic fission more acutely regulates synapse function has been unclear. Our relatively brief periods of suppressing fission had no effect on spine density, intrinsic electrophysiological properties, or basal transmission. However, fission was required for each classic aspect of LTP expression: dendritic spine growth, surface AMPAR trafficking, and potentiation of synaptic transmission. The lack of effect on basal transmission emphasizes the unforeseen and acute role of mitochondrial fission during LTP induction.

Several mechanisms could explain how an increase in fission may support LTP (Fig. 8H). First, LTP requires increased ATP synthesis (Kimura et al., 2012; Wieraszko, 1982), and Drp1 knockout reduces ATP synthesis (Oettinghaus et al., 2016; Shields et al., 2015), presumably by decreasing fission. Second, LTP may require an increase in ROS generation by dendritic mitochondria (Fu et al., 2017), perhaps to modulate spine actin dynamics (D'Ambrosi et al., 2014), and preventing fission decreases ROS generation in certain contexts (Hung et al., 2017; Kim et al., 2016; Qi et al., 2013). Third, fission could support LTP by modulating mitochondrial handling of dendritic Ca^{2+}. In physiological contexts, dendritic Ca^{2+} transients reflect the interplay of synaptic and dendritic NMDARs, voltage-gated Ca^{2+} channels, back-propagating action potentials, and intracellular Ca^{2+} sources (Higley and Sabatini, 2008; Linden, 1999). The temporal and spatial summation of synaptic inputs can thus result in supralinear Ca^{2+} increases over large extents of the dendrite (Dudman et al., 2007), linking active inputs with local plasticity (Carter et al., 2007; Major et al., 2008). LTP requires calcium-induced Ca^{2+} release (CICR) from internal stores, and the role of dendritic ER Ca^{2+} stores in plasticity has been extensively investigated

(Padamsey et al., 2018). However, mitochondria are also Ca^{2+} buffering organelles that participate in CICR (Ichas et al., 1997; Padamsey et al., 2018; Rizzuto et al., 2012), yet their role in LTP remains poorly understood.

Mitochondria permit Ca^{2+} into their matrix via the MCU (Rizzuto et al., 2012). Matrix Ca^{2+} can bind inorganic phosphate (Bielawski and Lehninger, 1966), can remain free to regulate metabolism, or can be released into the cytosol (Rizzuto et al., 2012). Interestingly, postsynaptic MCU activity is elevated during HFS-induced LTP induction in hippocampus (Stanton and Schanne, 1986), and inhibiting postsynaptic MCU impairs LTP of dorsal horn neurons (Kim et al., 2011). Consistent with this, we found that LTP induction prompts transient elevations of dendritic mitochondrial Ca^{2+}. Mitochondrial Ca^{2+} promotes ATP synthesis by activating several tricarboxylic acid cycle enzymes (Llorente-Folch et al., 2015), increases matrix ROS generation via the electron transport chain (Gorlach et al., 2015; Llorente-Folch et al., 2015), and may regulate CICR by transiently activating the mitochondrial permeability transition pore (Mnatsakanyan et al., 2017). Interestingly, these functions are similarly regulated by both mitochondrial fission and matrix Ca^{2+}, and consistent with this, we found that prohibiting mitochondrial fission suppresses mitochondrial Ca^{2+} handling. These data are consistent with previous findings in non-neuronal cells that smaller mitochondria tend to buffer Ca^{2+} faster whereas larger mitochondria have smaller amplitude and duration of evoked mitochondrial Ca^{2+} elevations (Bianchi et al., 2006; Szabadkai et al., 2004), though Drp1 knockout increases mitochondrial Ca^{2+} handling in macrophages (Wang et al., 2017), suggesting the need for further study. Taken together, it is possible that mitochondrial fission is required for LTP because it modulates mitochondrial Ca^{2+}, which in turn regulates one or more mitochondrial metabolic functions (Fig. 8H).

Additionally, because mitochondrial ATP synthesis, ROS generation, and Ca^{2+} handling are all interrelated and have bidirectional relationships with mitochondrial dynamics (Mishra and Chan, 2016; Szabadkai et al., 2006), it is important to consider the role of dendritic mitochondria in LTP and memory formation more broadly. Memory formation may require a combination of input-specific synaptic activation as well as a generalized elevation in local or global excitability of a dendrite or neuron, which would reduce the threshold for LTP induction (Lisman et al., 2018; Rogerson et al., 2014). As such, one possibility consistent with our results is that dendritic mitochondrial fission increases mitochondrial Ca^{2+} handling, thereby enhancing overall mitochondrial bioenergetic function and also regulating cytosolic Ca^{2+} patterns, both of which could not only maintain LTP at the activated synapse, but could also reduce the threshold for LTP at neighboring synapses on the same parent dendrite. In sum, there are diverse means by which mitochondrial fission could alter the threshold for plasticity at active synapses.

Given these considerations, it is tempting to speculate that local interaction of dendritic signaling with nearby mitochondria supports plasticity at appropriately activated synapses *in vivo.* Furthermore, clinically, missense mutations of Drp1 or Dyn2 (Bitoun et al., 2005; Flippo and Strack, 2017), and loss of function mutations of mitochondrial fission factor Mff (Koch et al., 2016), are associated with developmental delay, cognitive impairment, seizures, and other symptoms related to altered synaptic plasticity. Therefore, our results not only

suggest an essential role for dendritic mitochondrial fission in synaptic plasticity in physiological contexts, but also raise the important possibility that impaired mitochondrial fission plays a causal role in synaptic and cognitive deficits seen in neuropsychiatric diseases.

STAR METHODS

CONTACT FOR REAGENT AND RESOURCE SHARING

Further information and requests for resources and reagents should be directed to and will be fulfilled by the Lead Contact, Thomas A. Blanpied (TBlanpied@som.umaryland.edu).

EXPERIMENTAL MODEL AND SUBJECT DETAILS

All experimental protocols were approved by the University of Maryland School of Medicine Institutional Animal Care and Use Committee.

Primary neuronal culture—Dissociated hippocampal neurons from embryonic day 18 Sprague Dawley rats (both male and female) were prepared and plated on cleaned 18mm coverslips (Warner) as previously described (Frost et al., 2010). Briefly, coverslips were coated beforehand overnight at 37°C with poly-L-lysine (Sigma). Hippocampi were isolated, dissociated in trypsin and triturated, and cells were plated at 50k cells/coverslip in Neurobasal medium (Sigma) containing B27 (Gibco), glutaMAX1 (Gibco), 5% fetal bovine serum (Hyclone), and 1 μg/ml gentamycin (Cambrex). 24 hours later, the initial plating media was replaced with culture media lacking serum. Culture media supplemented with FUDR (10 μM) was added 1 week after plating to inhibit proliferation of non-neuronal cells. Cells were incubated at 37°C and 5% CO_2.

Acute hippocampal slices—Standard methods were used to prepare 400 μm-thick transverse hippocampal slices from 6-8-week-old mice (both male and female) as described previously (Cai et al., 2013). WT C57BL/6J or CaMKIIα-mitoEYFP (Chandrasekaran et al., 2006) mice were used. For field recordings, dissection was done in ice-cold artificial cerebrospinal fluid (ACSF) containing the following (in mM): 120 NaCl, 3 KCl, 1 NaH_2PO_4, 2 $MgSO_4$, 2.5 $CaCl_2$, 25 $NaHCO_3$, and 20 glucose, bubbled with 95% O_2/5% CO_2. Slices were allowed to recover for a minimum of 1 hour at room temperature (20–22°C). For whole-cell recordings, d issection was performed in cold N-methyl-D-glucamine ACSF (NMDG-ACSF) containing (in mM) 92 NMDG, 2.5 KCl, 1.25 NaH_2PO_4 30 $NaHCO_3$, 20 HEPES, 25 glucose, 0.5 $CaCl_2$, 10 $MgSO_4 \cdot 7H_2O$ and bubbled with carbogen (95% O_2-5% CO_2). Slices recovered for approximately 10 minutes in NMDG-ACSF at 32°C. Slices were then transferred to ACSF containing (in mM) 120 NaCl, 3 KCl, 1.0 NaH_2PO_4, 1.5 $MgSO_4 \cdot 7H_2O$, 2.5 $CaCl_2$, 25 $NaHCO_3$, and 20 glucose and bubbled with carbogen (95% O_2-5% CO_2) and recovered for one hour at 20–22°C.

METHOD DETAILS

Transfections—For most experiments, cells were transfected at DIV 17-19 using Lipofectamine 2000 (Invitrogen), with 0.5 μg/μL of DNA per plasmid, and imaged 4 days

later. For 10-day knockdown experiments, cells were transfected at DIV 11-13 and imaged 10 days later.

Reagents

Drugs and chemical compounds (in μM): D,L-APV (APV, 200, Sigma), picrotoxin (PTX, 50, Sigma), tetrodotoxin (TTX, 0.5, Millipore), strychnine (STR, 1, Sigma), glycine (Gly, 400, Sigma), Jasplakinolide (Jasp, 0.5, Invitrogen), Latrunculin A (Lat A, 10, Sigma), KN-93 (10, Millipore), KN-92 (10, Millipore), Mdivi-1 (10, Sigma), and CGP52432 (2, Tocris). For reagents solubilized in DMSO (Sigma), the final amount of DMSO was ≤0.1% by volume. MNI-Glutamate (Tocris) was prepared to a final concentration of 2 mM from single-use stock aliquots.

Antibodies: Primary: anti-Drp1 (rabbit, D6C7, CST, 1:50), anti-Homer1 (rabbit, Synaptic Systems,1:500), Anti-GluA2 (mouse, Millipore MAB397, 1:100). Secondary: Ax647 (Jackson Immuno) and Atto565 (Hypermol) conjugated goat or donkey anti-rabbit or anti-mouse secondary antibodies (1:200) were used.

Expression constructs: We thank the following individuals for donating published plasmid and virus constructs. GFP-Drp1, Mito-DsRed, and MitoRGeco were gifts from H. Higgs. GFP-Drp1DN was a gift from S. Strack. GFP-Dyn2 and GFP-Dyn2DN were gifts from P. Welling via P. De Camilli. SEP-GluA1 and SEP-GluA2 were gifts from R. Huganir. We thank T. Kristian for generously donating transgenic CaMKII-Mito-eYFP mice. GFP::Drp1-miRNA and GFP::Drp1-controlRNA were gifts from M.Lobo. AAV-*Cre*-YFPDrp1, AAV-*Cre*-YFPDrp1DN, and AAV-MitoDsRed were designed by R. Chandra and M. Lobo as previously described (Chandra et al., 2017). Briefly, Drp1DN (a gift from M. Karbowski) was PCR amplified and an EYFP tag was added to an AAV-DIO vector. Finally, virus packaging for AAV2-DIO-Drp1DN-EYFP (i.e. AAV-*Cre*-YFPDrp1DN) was performed as previously described (Chandra et al., 2015; Prasad et al., 2011). AAV2-Cre-GFP was purchased from UNC Vector Core by M. Lobo. Mito-DsRed vector was a gift from N.G. Larsson, and was similarly PCR amplified and cloned into a non-Cre dependent AAV vector.

Subcloning and mutagenesis: mCherry::Drp1-miRNA and mCherry::Drp1-controlRNA were generated from the original GFP:: variants (target sequences underlined below: 5'-3') using *in vitro* assembly (IVA) (Garcia-Nafria et al., 2016).

miRNA –

TGCTGGATGAACCGAAGAATAAGTTCGTTTTGGCCACTGACTGACGAACTTATTTCGGTTCATC

Control –

TGCTGGTAGTTGTACTCCAGCTTGTGGTTTTGGCCACTGACTGACCACAAGCTAGTACAACTAC

Briefly, the RNA-containing vector was PCR amplified using the following forward and reverse primers:

FW – GCCGTCGATCGTTTAAAGGGAG

REV – GGTTTTAAAGCCTGCTTTTTTGTACAAACT

mCherry DNA was PCR amplified using the following forward and reverse primers (5'-3'):

FW – GCAGGCTTTAAAACCATGGTGAGCAAGGGCGAGGA

REV – TAAACGATCGACGGCTACTTGTACAGCTCGTCCATGCC

PCR was performed using KAPA HiFi DNA polymerase (Kapa Biosystems). PCR reaction was treated with Dpn1 (New England Biolabs; NEB) enzyme to digest any original vector. 0.8% agarose gel electrophoresis was performed followed by gel extraction using a Gel DNA Recovery Kit (Zymo Research). The purified vector and insert were mixed together at a 1:1 molar ratio and transformed into NEB5α cells (NEB).

GFP-Drp1-S616A and -S616D were designed from GFP-Drp1 via site-directed mutagenesis using a commercially-available kit (Q5, NEB). Primers used were:

S616A-FW – TATGCCAGCAgctCCACAAAAAGGC

S616A-REV – ATTGGAATTGGTTTTGATTTTTC

S616D-FW – TATGCCAGCAgatCCACAAAAAGGC

S616D-REV – ATTGGAATTGGTTTTGATTTTTC

All subcloning was confirmed by sequencing.

Chemical LTP induction protocol—A protocol to chemically prompt activation of synaptic NMDARs to increase synaptic strength reliably in hippocampal cultures (cLTP) was refined (Araki et al., 2015; Liao et al., 1995). Briefly, neurons were transfected at DIV17-19, incubated in 200 μM APV 24 hrs later, and imaged 3 days later. Cells were preincubated for 1-4 hrs in extracellular solution containing 200 μM APV, 0.5 μM TTX, 1 μM STR, and 50 μM PTX. In structural LTP and mitochondrial fission experiments, 3 frames (5-minute interval = 1/300 Hz) were collected in basal solution, 3 frames after APV/Mg^{2+} withdrawal and simultaneous addition of 400 μM glycine, and 8 frames after wash-out. The negative control for cLTP stimulation was stimulation in the presence of APV (referred to in the text as +APV). In the mitochondrial fission/re-fusion experiment, following the 8 washout-frames, an additional 4 frames (15-minute interval) were collected. For Homer1-GluA2 immunocytochemistry experiments, cells were in each solution for the same amount of time and fixation was performed at the end of the wash-out period. In mitochondrial Ca^{2+} imaging experiments, 300 frames (100 ms exposure) were collected in basal solution, followed by 1800 frames in the stimulation solution.

Immunocytochemistry—Cells were fixed with 4% paraformaldehyde and 4% sucrose (PFA/Sucrose) in phosphate-buffered saline (PBS, pH 7.4) for 10 min at room temperature (RT), followed by three 10-min washes with 100 mM glycine in PBS (PBS/Gly). Cells were then permeabilized and blocked using 0.1% BSA and 5-10% donkey or goat serum in PBS/Gly with 0.1% Triton X-100, followed by incubation with primary antibody (3 hrs RT, or 4 °C overnight) and secondary antibodies (1 hr RT) that were diluted in blocking buffer

(without triton for secondary antibody solution). Coverslips were either imaged immediately or mounted onto slides using DABCO (Sigma) dissolved in Perma-Fluor (Thermo) for imaging the next day. To label surface synaptic AMPARs, a recently reported protocol (Wu et al., 2017) was followed. Briefly, neurons were fixed in PFA/Sucrose for 15 min on ice and immunostaining for GluA2 was performed without permeabilization. Following thorough washing in PBS/Gly, neurons were permeabilized and immunostained for Homer1. Secondary antibody labeling of both primary antibodies was then performed simultaneously.

Tissue Clearing—Tissue clearing was performed on hippocampal slices that were fixed in 4% PFA using a modified CUBIC approach (Susaki et al., 2014). Briefly, slices were placed in modified CUBIC Reagent-1A – 10%wt Triton, 5%wt NNNN-tetrakis (2-HP) ethylenediamine, 10%wt urea, and 1/200 volume 5 M NaCl (all Sigma) – that was diluted to 50% in dH2O, and gently shaken for 24 hrs at 37°C. The slices were then transferred and shaken in 100% Reagent-1A for another 24 - 48 hrs. Slices were then stored in Reagent-1A at 4°C prior to imaging.

Confocal microscopy

Cultured hippocampal neurons: Imaging was performed on two confocal microscopes. Data represented in Figures 1, S1A,E, 2B-C, S2, 5A-F, and S5A,H-J, were collected using a spinning disk CSU-22 confocal system (Andor, Yokogawa) and Zyla4.2 sCMOS camera (Andor), mounted onto an Olympus IX-81 inverted microscope. A 60x 1.42 NA oil-immersion objective (Olympus) was used for imaging, yielding a final effective pixel size of 108.3 nm. Laser illumination was provided using an Andor Laser Combiner (Andor), emission filters (Semrock), and motorized filter wheel (Sutter). To control for non-homogeneous illumination of the field-of-view in quantitative co-localization experiments, images were acquired from the same camera region. Data in Figures S1 B-D, 2A,D-I, S3, 3, 4, S4, 5G-J,S5B-G,K, 7, S7, and 8 were collected using an Andor Dragonfly spinning disk confocal system, which had a measured pixel size of 103.31 nm. Andor Borealis uniform illumination technology with the Dragonfly permitted quantitative co-localization experiments from the entire 2048 × 2048-pixel sCMOS field of view. For fission and structural LTP experiments, maximum intensity projections were acquired from 0.5 μm-step z-stacks of 7 planes (live cells) or 13 planes (fixed cells), using a piezoelectric z-focus device (Prior) to autofocus to the center plane, and 200 ms camera exposure per channel. For mitochondrial Ca^{2+} imaging experiments, a single z plane was imaged using continuous focus, 2×2 binning, and 100 ms camera exposure in the 561 nm excitation channel, with 300 baseline frames and 1800 post-stimulation frames. Before and after each timelapse, a 7-plane two-channel z-stack was acquired. Acquisition was controlled by iQ3.2 software (Andor). Live-cell imaging was performed in extracellular solution containing the following (in mM): NaCl (150), KCl (3), $MgCl_2$ (1), $CaCl_2$ (2), HEPES (10), D-glucose (10), pH 7.4, with temperature controlled by an objective collar heater (Bioptechs) set to 37 °C. For long-term imaging in mitochondrial fission/re-fusion experiments a customized Tokai-Hit CO2, temperature, and humidity-controlled chamber (Tokai Hit, STR-WELSX-IX3) was used.

Fixed and cleared acute hippocampal slices: Imaging for Fig. 6A,D was performed using an ORCA Flash4.0 sCMOS camera (Hamamatsu) mounted on a Nikon CSU-W1 spinning

disc confocal microscope system (Nikon) in the University of Maryland School of Medicine Confocal Core Facility. Low magnification images were acquired using a 4x air (0.2 NA, 20 mm WD), whereas high magnification imaging was performed with a 60x water-immersion (1.2 NA, 0.31 mm WD) objective with an effective pixel size of 108.3 nm that was loaned to us by W.J. Lederer. Slices were placed on glass-bottom 35 mm dishes (MatTek, #P35G-1.5-14-C) in CUBIC Reagent-1A. 100-μm z-stacks were collected using a 0.25 μm z-step size and 300 ms exposure with the 25 μm pinhole. The beginning of the z-stack was defined as ~75 μm from the bottom of the slice to avoid quantifying mitochondrial length in layers damaged during slicing. 3 stacks were collected per slice and the average mitochondrial length from the 3 regions was compared between groups.

Glutamate photolysis—Photolysis was performed using the Andor Dragonfly and FRAPPA systems. MNI-glutamate was kept protected from ambient light and was applied (2 mM) to coverslips only after finding cells that displayed spontaneous activity in the presence of TTX. A 60 second train of 500 μs, 405 nm laser pulses at 1 Hz was used for photolysis, similar to reported protocols (Chang et al., 2017; Fu et al., 2017; Sinnen et al., 2017). Images were acquired as a combination of z-stacks for both MitoDsRed and GCaMP6f, and single-plane time-series for GCaMP6f alone, using a piezoelectric center z autofocus device, with 50 ms camera exposure.

Stereotactic injections—Injections were performed as previously described (Chandra et al., 2017). Briefly, mice were anesthetized using 4% isoflurane in a small induction chamber. After the initial induction, isoflurane was maintained at 1% for the remainder of the surgery. Animals were placed in a stereotaxic instrument and their skull was exposed. 33-gauge Hamilton syringe needles were used to inject 0.6 μl of: AAV-MitoDsRed, AAV-*Cre*-GFP, and either AAV-*Cre*-YFPDrp1 or AAV-*Cre*-YFPDrp1DN bilaterally into area CA1 of hippocampus (in relation to bregma: anterior/posterior, −2.5 mm; medial/lateral, ±1.5 mm; dorsal/ventral, −1.3 mm; 10° angle). Mice were then returned to the vivarium for 2-3 weeks to allow for recovery and maximal virus expression.

Acute slice electrophysiology

Field EPSP recordings: Standard methods were used to prepare 400μm-thick transverse hippocampal slices from 6-8-week-old mice as described previously (Cai et al., 2013; Kallarackal et al., 2013). Briefly, dissection was done in ice-cold artificial cerebrospinal fluid (ACSF) containing the following (in mM): 120 NaCl, 3 KCl, 1 NaH_2PO_4, 2 $MgSO_4$, 2.5 $CaCl_2$, 25 $NaHCO_3$, and 20 glucose, bubbled with 95% O_2/5% CO_2. Slices were allowed to recover for a minimum of 1 hour at room temperature (20–22°C). Slices were then examined, using a fluorescence microscope, for the expression and accuracy of the viral injections. Only slices that displayed virus expression in CA1 alone were used in the study. Next, slices were transferred to a submersion-type recording chamber and perfused with ACSF. The CA2/CA3 region was then removed to sever reciprocal connections and prevent spontaneous epileptiform discharge. Picrotoxin (100μM) and CGP52432 (2μM) were included during recording to block $GABA_A$ and $GABA_B$ receptors, respectively.

Extracellular recording of local field excitatory postsynaptic potentials (fEPSPs) was performed to assess the synaptic strength of Schaffer collateral connections (SC-CA1). Recording pipettes containing ACSF (3–5 MΩ) were placed 100–150μm from the concentric bipolar tungsten stimulating electrodes in the *stratum radiatum* to record SC-CA1 responses. fEPSPs were recorded using n.p.i. (NPI) amplifiers amplified 1000x, filtered at 3 kHz, and digitized at 10 kHz.

Basal transmission was assessed by delivering stimuli (100 μs; 0.05 Hz) of increasing intensity to assess synaptic transmission over a broad range of responses. The amplitude of the fiber volley (FV) was used as an indicator of stimulus intensity and normalization of a response to its FV allowed for direct comparison from different stimuli. Six consecutive responses were averaged and the initial slope of the first 1.8-2 ms was used an indicator of the strength of the AMPA receptor-mediated component of the evoked response.

Stimulus intensity was then set at 150% of threshold intensity, resulting in a fEPSP of 0.1–0.2 mV. Responses were binned into minute averages and fEPSPs were elicited for a >30 min baseline period to ensure stable responses prior to the induction of LTP using a high frequency stimulation protocol (HFS; 4 trains of 100 pulses delivered at 100 Hz; 1 min inter-train interval). Stimulation was then resumed at 0.05 Hz for the duration of the experiment.

Whole-cell recordings: Hippocampal dissection was performed in cold N-methyl-D-glucamine artificial cerebrospinal fluid (NMDG-ACSF) containing (in mM) 92 NMDG, 2.5 KCl, 1.25 NaH_2PO_4, 30 $NaHCO_3$, 20 HEPES, 25 glucose, 0.5 $CaCl_2$, 10 $MgSO_4 \cdot 7H_2O$ and bubbled with carbogen (95% O_2-5% CO_2). Slices recovered for approximately 10 minutes in NMDG-ACSF at 32. Slices were then transferred to ACSF containing (in mM) 120 NaCl, 3 KCl, 1.0 NaH_2PO_4, 1.5 $MgSO_4 \cdot 7H_2O$, 2.5 $CaCl_2$, 25 $NaHCO_3$, and 20 glucose and bubbled with carbogen (95% O_2-5% CO_2) and recovered for one hour at 20–22°C. They were then transferred to a submersion-type chamber for recording and superfused at 20–22°C (flow rate 0.5–1 ml/min).

Cells were visualized under differential interference contrast using a 60x water immersion objective (Nikon Eclipse E600FN). Infected CA1 cells were identified by their expression of YFP.

Whole-cell current clamp recordings were obtained using an Axopatch 200B amplifier (Axon Instruments, Union City, CA) and digitized with a Digidata 1440 analog-digital converter (Instrutech, Elmont, NY). Patch pipettes were pulled to resistances of 3-8MΩ. Patch pipettes were filled with a solution containing 130mM K-gluconate, 5mM KCl, 2mM $MgCl_2$-6H2O, 10mM HEPES, 4 mM Mg-ATP, 0.3mM Na_2-GTP, 10mM Na_2-phosphocreatine, and 1mM EGTA. The extracellular solution consisted of ASCF and 50μM picrotoxin. Input resistance was calculated by delivering a series of hyperpolarizing current steps to pyramidal neurons (−50 pA for approximately 500ms) and measuring the voltage deflection. The maximum firing rate of neurons was determined by delivering increasing depolarizing current steps and calculating the maximum frequency at which the cells could fire faithfully. Action potential threshold was measured by delivering a ramp of depolarizing current to cells, and the voltage at which the first action potential fired was recorded.

QUANTIFICATION AND STATISTICAL ANALYSIS

Experimental design and quantification—Experiments were performed with the investigators blinded to experimental conditions (e.g. expression construct, stimulation, inhibitor, animal, etc.). The blind was not broken until data analysis was complete.

Mitochondrial length and dendrite length were measured using Mytoe (Lihavainen et al., 2012), and ImageJ plugin NeuronJ (Meijering et al., 2004), respectively. In all experiments, secondary to quaternary dendrites were analyzed because primary dendrites have too high mitochondrial density to be spatially resolved, whereas much higher-order dendrites had too scarce mitochondria. Dendritic spine density was performed by counting the number of spines and dividing by the length of dendrite. This was done in ImageJ by a second investigator who was blinded to the experimental conditions. To compare basal spine size, spine area was measured using automated threshold-based integrated morphometry analysis in MetaMorph (Molecular Devices). Here, area was used in lieu of intensity in order to control for differences in fluorescent protein expression levels between cells. To compare structural changes during LTP, spine volume, area, and surface AMPAR data were analyzed using ImageJ and custom-written MetaMorph journals and Matlab (MathWorks) scripts. Briefly, drift and movement were first corrected for using the ImageJ plugin StackReg (Thevenaz et al., 1998). Then, regions of interest (ROIs) around spines were blindly selected, and background-subtracted integrated intensity of membrane-mCherry, membrane-mRuby, or SEP-GluA1,2 fluorescence was measured using automated MetaMorph journals. Only spines that remained within the ROI for the duration of imaging were used. Post hoc, data were normalized to the average of the first three baseline frames within each ROI using Matlab. Baseline subtraction using a negative control was performed in Prism (GraphPad) to account for mem-mCherry and -mRuby photobleaching.

Mitochondrial fission events were counted frame by frame using ImageJ, while blinded, similar to previous strategies (Ji et al., 2015; Li et al., 2004). The number of fission events was normalized to the dendrite length in which fission was analyzed, which range ranged from 3000-16000 μm per group in cLTP experiments. The change in fission events was calculated by subtracting the average of the number of fission events in two baseline points from the point immediately after stimulation, during which the burst of fission occurred. When baseline fission is reported, the bar graphs represent the average fission of the first two baseline points, analyzed from the first three baseline frames. In glutamate photolysis experiments, the length of dendrite analyzed was less, ~1000 μm per group, since only regions exhibiting an increase in GCaMP6f ΔF/F could be used and because a randomly-selected dendritic segment of a similar length was selected from the same cell as a negative control. The distance between sites of mitochondrial fission and dendritic spines on the same dendrite branch that had undergone LTP was measured by first identifying single point ROIs at the dendritic shaft base of structurally potentiated spines in ImageJ while blinded to the mitochondrial signal. Then, mitochondrial fission events were identified as above and another single point ROI was used to label the fission spot, and point-to-point distance was measured using the line tool. An upper limit for the distance was set at 50 μm and only the nearest mitochondrial fission site to a given potentiated spine was reported. For

mitochondrial re-fusion, cLTP fission burst events were identified and the timecourse of re-fusion of these fission events was determined.

For Drp1 immunocytochemistry quantification using ImageJ, ROIs were drawn while visualizing GFP fluorescence and blinded to Ax647 fluorescence, which was measured. Surface synaptic AMPAR intensity was quantified in MetaMorph. ROIs were drawn using automated thresholding of Homer1 to demarcate the synapse while blinded to GluA2 data. Then, the average GluA2 intensity within a Homer1 mask-defined ROI was measured.

For analysis of GCaMP6f intensity, ROIs were drawn around thresholded masks of averaged images using custom-written automated MetaMorph journals. ΔF/F was calculated in Matlab as $(F_{end} - F_{beginning})/F_{beginning}$, where F_{end} was measured from the averaged image of the last 200 frames after stimulation and $F_{beginning}$ was measured from the averaged image of the first 200 frames before stimulation. The color map was made using ImageJ.

For electrophysiological LTP experiments, fEPSP slope values were averaged and quantified over a 3 min period preceding HFS, and a 3 min period at the end of the manipulation. fEPSP values were quantified relative to the average value of the 10-minute baseline period immediately preceding the first manipulation. To analyze the AMPAR-mediated responses, the window was fixed in the initial rising phase of the response, 2–5 ms after its initiation. Mitochondrial length in the hippocampal slice LTP experiment was normalized to the pooled average of the mean mitochondrial lengths from each slice in both groups. Slices in which APV treatment failed to return the fEPSP slope to baseline (defined by at least less than 10% increase from the baseline average) were excluded from analysis. All LTP recordings and slice imaging were performed by separate investigators who were blinded to experimental conditions.

Analysis of mitochondrial Ca^{2+} was performed as follows. First, an average intensity projection of the baseline frames was created, followed by background subtraction in ImageJ. Next, an intensity-based mask of individual mitochondria was automatically created in MetaMorph. Average intensity values within mitochondrial regions defined by this mask were then collected from the Mito-RGECO timeseries in MetaMorph and underwent background subtraction based on a background region in Matlab. ΔF/F (i.e. $(F- F_0)/F_0$) was then calculated in Matlab, in which F was defined as the average intensity value and F_0 was iteratively calculated every 600 frames from the average of the smallest 5 average intensity values, to account for photobleaching. Traces with excessive noise or large ΔF/F values were filtered out. Events from the remaining sweeps were detected in Clampfit (Molecular Devices) by hand while blinded, using Threshold Search. These data were then compiled in Matlab prior to statistical analysis in Prism.

Statistics

Statistics for all experiments were performed using GraphPad Prism and all figures were prepared using Microsoft PowerPoint. Most statistical details of experiments – including n, what n represents, dispersion and precision measures, etc. – can be found in the Results section. Significance was defined as $p < 0.05$ and all p values are reported. Statistical tests used are described here to avoid redundancy in the text. Briefly, column statistics were first

performed and a D'Agostino-Pearson omnibus normality test was used to determine whether the sample values were likely from a Gaussian distribution. If so, the appropriate parametric test without assuming equal variance was used, and if not, the appropriate non-parametric test was used. Pearson and Spearman analyses were performed for correlations and are reported in the main text. For analysis of two groups, either a parametric t-test with Welch's correction or a non-parametric Mann-Whitney test was performed. For analysis of two groups in the photolysis experiment, a paired t-test was used since data in the control and experimental groups were both acquired from the same cell, simultaneously. For analysis of distributions, a Kolmogorov-Smirnov test was used. For analysis of three or more groups across one factor, One-way ANOVA (either ordinary or Kruskal-Wallis) was performed, with a post hoc Dunn's test only if significant. The reported post hoc value is with respect to the mentioned control. For comparison of two or more factors (e.g. time and stimulation, expression construct and time, etc.), a Two-way ANOVA was performed, and post hoc test (either Sidak, Dunnett, or Tukey, as recommended) for multiple comparisons was performed only if the interaction p-value and/or the p-value of the factor of interest were significant. For Two-way ANOVA, several p-values are clearly reported in the main text for each experiment including for the interaction, factor of interest, and post hoc comparison.

Supplementary Material

Refer to Web version on PubMed Central for supplementary material.

ACKNOWLEDGEMENTS

We sincerely thank members of the Scott Thompson, Mary Kay Lobo, Henry Higgs, Alexandros Poulopoulos, and David Benavides labs for helpful discussions, and Brian Polster and members of the Blanpied lab for also critically evaluating the manuscript. We thank Wei-ke Ji for advice on fission analysis, Sarah Metzbower for advice on calcium imaging analysis, Alexandros Poulopoulos and Andrea Romanowski for help with tissue clearing, Tibor Kristian for providing MitoEYFP mice, Michel Engeln for advice on stereotactic injections, W. Jon Lederer for loaning us a 60x water-immersion objective, and Humberto Joca for help with testing slice imaging configurations. We thank the following for generously sharing expression constructs: GFPDrp1DN (Stefan Strack), GFPDyn2 and Dyn2DN (Paul A. Welling and Pietro De Camilli), SEP-GluA1 and GluA2 (Richard L. Huganir). This work was supported by the NIH (F30 MH111207 and T32 NS063391 to S.S.D., T32 GM008181 to P.A.D., and R01s GM106000 to H.N.H. and T.A.B., MH080046 to T.A.B., MH086828 to S.M.T., and DA038613 to M.K.L.), a NARSAD Young Investigator award to T.A.L., and the Kahlert Foundation to T.A.B.

REFERENCES

Araki Y, Zeng M, Zhang M, and Huganir RL (2015). Rapid dispersion of SynGAP from synaptic spines triggers AMPA receptor insertion and spine enlargement during LTP. Neuron 85, 173–189. [PubMed: 25569349]

Archer SL (2013). Mitochondrial dynamics--mitochondrial fission and fusion in human diseases. The New England journal of medicine 369, 2236–2251. [PubMed: 24304053]

Basu K, Lajoie D, Aumentado-Armstrong T, Chen J, Koning RI, Bossy B, Bostina M, Sik A, Bossy-Wetzel E, and Rouiller I (2017). Molecular mechanism of DRP1 assembly studied in vitro by cryo-electron microscopy. PloS one 12, e0179397. [PubMed: 28632757]

Bianchi K, Vandecasteele G, Carli C, Romagnoli A, Szabadkai G, and Rizzuto R (2006). Regulation of Ca2+ signalling and Ca2+-mediated cell death by the transcriptional coactivator PGC-1alpha. Cell Death Differ 13, 586–596. [PubMed: 16239931]

Bielawski J, and Lehninger AL (1966). Stoichiometric relationships in mitochondrial accumulation of calcium and phosphate supported by hydrolysis of adenosine triphosphate. The Journal of biological chemistry 241, 4316–4322. [PubMed: 4162498]

Bitoun M, Maugenre S, Jeannet PY, Lacene E, Ferrer X, Laforet P, Martin JJ, Laporte J, Lochmuller H, Beggs AH, et al. (2005). Mutations in dynamin 2 cause dominant centronuclear myopathy. Nat Genet 37, 1207–1209. [PubMed: 16227997]

Bordt EA, Clerc P, Roelofs BA, Saladino AJ, Tretter L, Adam-Vizi V, Cherok E, Khalil A, Yadava N, Ge SX, et al. (2017). The Putative Drp1 Inhibitor mdivi-1 Is a Reversible Mitochondrial Complex I Inhibitor that Modulates Reactive Oxygen Species. Developmental cell 40, 583–594 e586. [PubMed: 28350990]

Cai X, Kallarackal AJ, Kvarta MD, Goluskin S, Gaylor K, Bailey AM, Lee HK, Huganir RL, and Thompson SM (2013). Local potentiation of excitatory synapses by serotonin and its alteration in rodent models of depression. Nat Neurosci 16, 464–472. [PubMed: 23502536]

Carroll RC, Beattie EC, Xia H, Luscher C, Altschuler Y, Nicoll RA, Malenka RC, and von Zastrow M (1999). Dynamin-dependent endocytosis of ionotropic glutamate receptors. Proceedings of the National Academy of Sciences of the United States of America 96, 14112–14117. [PubMed: 10570207]

Carter AG, Soler-Llavina GJ, and Sabatini BL (2007). Timing and location of synaptic inputs determine modes of subthreshold integration in striatal medium spiny neurons. The Journal of neuroscience : the official journal of the Society for Neuroscience 27, 8967–8977. [PubMed: 17699678]

Cassidy-Stone A, Chipuk JE, Ingerman E, Song C, Yoo C, Kuwana T, Kurth MJ, Shaw JT, Hinshaw JE, Green DR, et al. (2008). Chemical inhibition of the mitochondrial division dynamin reveals its role in Bax/Bak-dependent mitochondrial outer membrane permeabilization. Developmental cell 14, 193–204. [PubMed: 18267088]

Chakrabarti R, Ji WK, Stan RV, de Juan Sanz J, Ryan TA, and Higgs HN (2018). INF2-mediated actin polymerization at the ER stimulates mitochondrial calcium uptake, inner membrane constriction, and division. The Journal of cell biology 217, 251–268. [PubMed: 29142021]

Chandra R, Engeln M, Schiefer C, Patton MH, Martin JA, Werner CT, Riggs LM, Francis TC, McGlincy M, Evans B et al. (2017). Drp1 Mitochondrial Fission in D1 Neurons Mediates Behavioral and Cellular Plasticity during Early Cocaine Abstinence. Neuron 96, 1327–1341 e1326. [PubMed: 29268097]

Chandra R, Francis TC, Konkalmatt P, Amgalan A, Gancarz AM, Dietz DM, and Lobo MK (2015). Opposing role for Egr3 in nucleus accumbens cell subtypes in cocaine action. The Journal of neuroscience : the official journal of the Society for Neuroscience 35, 7927–7937. [PubMed: 25995477]

Chandrasekaran K, Hazelton JL, Wang Y, Fiskum G, and Kristian T (2006). Neuron-specific conditional expression of a mitochondrially targeted fluorescent protein in mice. The Journal of neuroscience : the official journal of the Society for Neuroscience 26, 13123–13127. [PubMed: 17182763]

Chang JY, Parra-Bueno P, Laviv T, Szatmari EM, Lee SR, and Yasuda R (2017). CaMKII Autophosphorylation Is Necessary for Optimal Integration of Ca2+ Signals during LTP Induction, but Not Maintenance. Neuron 94, 800–808.e804. [PubMed: 28521133]

Cho B, Cho HM, Jo Y, Kim HD, Song M, Moon C, Kim H, Kim K, Sesaki H, Rhyu IJ, et al. (2017). Constriction of the mitochondrial inner compartment is a priming event for mitochondrial division. Nature communications 8, 15754.

Cho B, Cho HM, Kim HJ, Jeong J, Park SK, Hwang EM, Park JY, Kim WR, Kim H, and Sun W (2014). CDK5-dependent inhibitory phosphorylation of Drp1 during neuronal maturation. Exp Mol Med 46, e105. [PubMed: 25012575]

D'Ambrosi N, Rossi S, Gerbino V, and Cozzolino M (2014). Rac1 at the crossroad of actin dynamics and neuroinflammation in Amyotrophic Lateral Sclerosis. Front Cell Neurosci 8, 279. [PubMed: 25249940]

Dudman JT, Tsay D, and Siegelbaum SA (2007). A role for synaptic inputs at distal dendrites: instructive signals for hippocampal long-term plasticity. Neuron 56, 866–879. [PubMed: 18054862]

Faits MC, Zhang C, Soto F, and Kerschensteiner D (2016). Dendritic mitochondria reach stable positions during circuit development. eLife 5, e11583. [PubMed: 26742087]

Ferguson SM, and De Camilli P (2012). Dynamin, a membrane-remodelling GTPase. Nature reviews Molecular cell biology 13, 75–88. [PubMed: 22233676]

Flippo KH, and Strack S (2017). Mitochondrial dynamics in neuronal injury, development and plasticity. Journal of cell science 130, 671–681. [PubMed: 28154157]

Frost NA, Shroff H, Kong H, Betzig E, and Blanpied TA (2010). Single-molecule discrimination of discrete perisynaptic and distributed sites of actin filament assembly within dendritic spines. Neuron 67, 86–99. [PubMed: 20624594]

Fu ZX, Tan X, Fang H, Lau PM, Wang X, Cheng H, and Bi GQ (2017). Dendritic mitoflash as a putative signal for stabilizing long-term synaptic plasticity. Nature communications 8, 31.

Garcia-Nafria J, Watson JF, and Greger IH (2016). IVA cloning: A single-tube universal cloning system exploiting bacterial In Vivo Assembly. Sci Rep 6, 27459. [PubMed: 27264908]

Godoy JA, Arrazola MS, Ordenes D, Silva-Alvarez C, Braidy N, and Inestrosa NC (2014). Wnt-5a ligand modulates mitochondrial fission-fusion in rat hippocampal neurons. The Journal of biological chemistry 289, 36179–36193. [PubMed: 25336659]

Gorlach A, Bertram K, Hudecova S, and Krizanova O (2015). Calcium and ROS: A mutual interplay. Redox Biol 6, 260–271. [PubMed: 26296072]

Harris JJ, Jolivet R, and Attwell D (2012). Synaptic energy use and supply. Neuron 75, 762–777. [PubMed: 22958818]

Hatch AL, Gurel PS, and Higgs HN (2014). Novel roles for actin in mitochondrial fission. Journal of cell science 127, 4549–4560. [PubMed: 25217628]

Hatch AL, Ji WK, Merrill RA, Strack S, and Higgs HN (2016). Actin filaments as dynamic reservoirs for Drp1 recruitment. Molecular biology of the cell 27, 3109–3121. [PubMed: 27559132]

Higley MJ, and Sabatini BL (2008). Calcium signaling in dendrites and spines: practical and functional considerations. Neuron 59, 902–913. [PubMed: 18817730]

Hung CH, Cheng SS, Cheung YT, Wuwongse S, Zhang NQ, Ho YS, Lee SM, and Chang RC (2017). A reciprocal relationship between reactive oxygen species and mitochondrial dynamics in neurodegeneration. Redox Biol 14, 7–19. [PubMed: 28837882]

Ichas F, Jouaville LS, and Mazat JP (1997). Mitochondria are excitable organelles capable of generating and conveying electrical and calcium signals. Cell 89, 1145–1153. [PubMed: 9215636]

Ishihara N, Nomura M, Jofuku A, Kato H, Suzuki SO, Masuda K, Otera H, Nakanishi Y, Nonaka I, Goto Y, et al. (2009). Mitochondrial fission factor Drp1 is essential for embryonic development and synapse formation in mice. Nat Cell Biol 11, 958–966. [PubMed: 19578372]

Jaskolski F, Mayo-Martin B, Jane D, and Henley JM (2009). Dynamin-dependent membrane drift recruits AMPA receptors to dendritic spines. The Journal of biological chemistry 284, 12491–12503. [PubMed: 19269965]

Ji WK, Hatch AL, Merrill RA, Strack S, and Higgs HN (2015). Actin filaments target the oligomeric maturation of the dynamin GTPase Drp1 to mitochondrial fission sites. eLife 4, e11553. [PubMed: 26609810]

Jiang HC, Hsu JM, Yen CP, Chao CC, Chen RH, and Pan CL (2015). Neural activity and CaMKII protect mitochondria from fragmentation in aging Caenorhabditis elegans neurons. Proceedings of the National Academy of Sciences of the United States of America 112, 8768–8773. [PubMed: 26124107]

Kallarackal AJ, Kvarta MD, Cammarata E, Jaberi L, Cai X, Bailey AM, and Thompson SM (2013). Chronic stress induces a selective decrease in AMPA receptor-mediated synaptic excitation at hippocampal temporoammonic-CA1 synapses. The Journal of neuroscience : the official journal of the Society for Neuroscience 33, 15669–15674. [PubMed: 24089474]

Kim DI, Lee KH, Gabr AA, Choi GE, Kim JS, Ko SH, and Han HJ (2016). Abeta-Induced Drp1 phosphorylation through Akt activation promotes excessive mitochondrial fission leading to neuronal apoptosis. Biochimica et biophysica acta 1863, 2820–2834. [PubMed: 27599716]

Kim HY, Lee KY, Lu Y, Wang J, Cui L, Kim SJ, Chung JM, and Chung K (2011). Mitochondrial Ca(2+) uptake is essential for synaptic plasticity in pain. The Journal of neuroscience : the official journal of the Society for Neuroscience 31, 12982–12991. [PubMed: 21900577]

Kimura R, Ma LY, Wu C, Turner D, Shen JX, Ellsworth K, Wakui M, Maalouf M, and Wu J (2012). Acute exposure to the mitochondrial complex I toxin rotenone impairs synaptic long-term potentiation in rat hippocampal slices. CNS Neurosci Ther 18, 641–646. [PubMed: 22613619]

Koch J, Feichtinger RG, Freisinger P, Pies M, Schrodl F, Iuso A, Sperl W, Mayr JA, Prokisch H, and Haack TB (2016). Disturbed mitochondrial and peroxisomal dynamics due to loss of MFF causes Leigh-like encephalopathy, optic atrophy and peripheral neuropathy. J Med Genet 53, 270–278. [PubMed: 26783368]

Korobova F, Gauvin TJ, and Higgs HN (2014). A role for myosin II in mammalian mitochondrial fission. Current biology : CB 24, 409–414. [PubMed: 24485837]

Korobova F, Ramabhadran V, and Higgs HN (2013). An actin-dependent step in mitochondrial fission mediated by the ER-associated formin INF2. Science (New York, NY) 339, 464–467.

Lee JE, Westrate LM, Wu H, Page C, and Voeltz GK (2016). Multiple dynamin family members collaborate to drive mitochondrial division. Nature 540, 139–143. [PubMed: 27798601]

Li Z, Okamoto K, Hayashi Y, and Sheng M (2004). The importance of dendritic mitochondria in the morphogenesis and plasticity of spines and synapses. Cell 119, 873–887. [PubMed: 15607982]

Liao D, Hessler NA, and Malinow R (1995). Activation of postsynaptically silent synapses during pairing-induced LTP in CA1 region of hippocampal slice. Nature 375, 400–404. [PubMed: 7760933]

Lihavainen E, Makela J, Spelbrink JN, and Ribeiro AS (2012). Mytoe: automatic analysis of mitochondrial dynamics. Bioinformatics 28, 1050–1051. [PubMed: 22321700]

Linden DJ (1999). The return of the spike: postsynaptic action potentials and the induction of LTP and LTD. Neuron 22, 661–666. [PubMed: 10230787]

Lisman J, Cooper K, Sehgal M, and Silva AJ (2018). Memory formation depends on both synapse-specific modifications of synaptic strength and cell-specific increases in excitability. Nat Neurosci 21, 309–314. [PubMed: 29434376]

Lisman J, Yasuda R, and Raghavachari S (2012). Mechanisms of CaMKII action in long-term potentiation. Nature reviews Neuroscience 13, 169–182. [PubMed: 22334212]

Llorente-Folch I, Rueda CB, Pardo B, Szabadkai G, Duchen MR, and Satrustegui J (2015). The regulation of neuronal mitochondrial metabolism by calcium. The Journal of physiology 593, 3447–3462. [PubMed: 25809592]

Major G, Polsky A, Denk W, Schiller J, and Tank DW (2008). Spatiotemporally graded NMDA spike/plateau potentials in basal dendrites of neocortical pyramidal neurons. Journal of neurophysiology 99, 2584–2601. [PubMed: 18337370]

Manor U, Bartholomew S, Golani G, Christenson E, Kozlov M, Higgs H, Spudich J, and Lippincott-Schwartz J (2015). A mitochondria-anchored isoform of the actin-nucleating spire protein regulates mitochondrial division. eLife 4.

Meijering E, Jacob M, Sarria JC, Steiner P, Hirling H, and Unser M (2004). Design and validation of a tool for neurite tracing and analysis in fluorescence microscopy images. Cytometry A 58, 167–176. [PubMed: 15057970]

Merrill RA, Dagda RK, Dickey AS, Cribbs JT, Green SH, Usachev YM, and Strack S (2011). Mechanism of neuroprotective mitochondrial remodeling by PKA/AKAP1. PLoS Biol 9, e1000612. [PubMed: 21526220]

Misgeld T, and Schwarz TL (2017). Mitostasis in Neurons: Maintaining Mitochondria in an Extended Cellular Architecture. Neuron 96, 651–666. [PubMed: 29096078]

Mishra P, and Chan DC (2016). Metabolic regulation of mitochondrial dynamics. The Journal of cell biology 212, 379–387. [PubMed: 26858267]

Mnatsakanyan N, Beutner G, Porter GA, Alavian KN, and Jonas EA (2017). Physiological roles of the mitochondrial permeability transition pore. J Bioenerg Biomembr 49, 13–25. [PubMed: 26868013]

Nicoll RA (2017). A Brief History of Long-Term Potentiation. Neuron 93, 281–290. [PubMed: 28103477]

Oettinghaus B, Schulz JM, Restelli LM, Licci M, Savoia C, Schmidt A, Schmitt K, Grimm A, More L, Hench J, et al. (2016). Synaptic dysfunction, memory deficits and hippocampal atrophy due to ablation of mitochondrial fission in adult forebrain neurons. Cell Death Differ 23, 18–28. [PubMed: 25909888]

Okamoto K, Bosch M, and Hayashi Y (2009). The roles of CaMKII and F-actin in the structural plasticity of dendritic spines: a potential molecular identity of a synaptic tag? Physiology (Bethesda) 24, 357–366. [PubMed: 19996366]

Padamsey Z, Foster WJ, and Emptage NJ (2018). Intracellular Ca(2+) Release and Synaptic Plasticity: A Tale of Many Stores. The Neuroscientist : a review journal bringing neurobiology, neurology and psychiatry, 1073858418785334.

Pagliuso A, Cossart P, and Stavru F (2017). The ever-growing complexity of the mitochondrial fission machinery. Cellular and molecular life sciences : CMLS.

Prasad KM, Smith RS, Xu Y, and French BA (2011). A single direct injection into the left ventricular wall of an adeno-associated virus 9 (AAV9) vector expressing extracellular superoxide dismutase from the cardiac troponin-T promoter protects mice against myocardial infarction. J Gene Med 13, 333–341. [PubMed: 21674736]

Qi X, Qvit N, Su YC, and Mochly-Rosen D (2013). A novel Drp1 inhibitor diminishes aberrant mitochondrial fission and neurotoxicity. Journal of cell science 126, 789–802. [PubMed: 23239023]

Rizzuto R, De Stefani D, Raffaello A, and Mammucari C (2012). Mitochondria as sensors and regulators of calcium signalling. Nature reviews Molecular cell biology 13, 566–578. [PubMed: 22850819]

Rogerson T, Cai DJ, Frank A, Sano Y, Shobe J, Lopez-Aranda MF, and Silva AJ (2014). Synaptic tagging during memory allocation. Nature reviews Neuroscience 15, 157–169. [PubMed: 24496410]

Rosenbloom AB, Lee SH, To M, Lee A, Shin JY, and Bustamante C (2014). Optimized two-color super resolution imaging of Drp1 during mitochondrial fission with a slow-switching Dronpa variant. Proceedings of the National Academy of Sciences of the United States of America 111, 13093–13098. [PubMed: 25149858]

Sheng ZH, and Cai Q (2012). Mitochondrial transport in neurons: impact on synaptic homeostasis and neurodegeneration. Nature reviews Neuroscience 13, 77–93. [PubMed: 22218207]

Shields LY, Kim H, Zhu L, Haddad D, Berthet A, Pathak D, Lam M, Ponnusamy R, Diaz-Ramirez LG, Gill TM, et al. (2015). Dynamin-related protein 1 is required for normal mitochondrial bioenergetic and synaptic function in CA1 hippocampal neurons. Cell Death Dis 6, e1725. [PubMed: 25880092]

Sinnen BL, Bowen AB, Forte JS, Hiester BG, Crosby KC, Gibson ES, Dell'Acqua ML, and Kennedy MJ (2017). Optogenetic Control of Synaptic Composition and Function. Neuron 93, 646–660.e645. [PubMed: 28132827]

Smirnova E, Griparic L, Shurland DL, and van der Bliek AM (2001). Dynamin-related protein Drp1 is required for mitochondrial division in mammalian cells. Molecular biology of the cell 12, 2245–2256. [PubMed: 11514614]

Stanton PK, and Schanne FA (1986). Hippocampal long-term potentiation increases mitochondrial calcium pump activity in rat. Brain research 382, 185–188. [PubMed: 2945618]

Susaki EA, Tainaka K, Perrin D, Kishino F, Tawara T, Watanabe TM, Yokoyama C, Onoe H, Eguchi M, Yamaguchi S, et al. (2014). Whole-brain imaging with single-cell resolution using chemical cocktails and computational analysis. Cell 157, 726–739. [PubMed: 24746791]

Szabadkai G, Simoni AM, Bianchi K, De Stefani D, Leo S, Wieckowski MR, and Rizzuto R (2006). Mitochondrial dynamics and Ca2+ signaling. Biochimica et biophysica acta 1763, 442–449. [PubMed: 16750865]

Szabadkai G, Simoni AM, Chami M, Wieckowski MR, Youle RJ, and Rizzuto R (2004). Drp-1-dependent division of the mitochondrial network blocks intraorganellar Ca2+ waves and protects against Ca2+-mediated apoptosis. Mol Cell 16, 59–68. [PubMed: 15469822]

Thevenaz P, Ruttimann UE, and Unser M (1998). A pyramid approach to subpixel registration based on intensity. IEEE Trans Image Process 7, 27–41. [PubMed: 18267377]

Todorova V, and Blokland A (2017). Mitochondria and Synaptic Plasticity in the Mature and Aging Nervous System. Curr Neuropharmacol 15, 166–173. [PubMed: 27075203]

Wakabayashi J, Zhang Z, Wakabayashi N, Tamura Y, Fukaya M, Kensler TW, Iijima M, and Sesaki H (2009). The dynamin-related GTPase Drp1 is required for embryonic and brain development in mice. The Journal of cell biology 186, 805–816. [PubMed: 19752021]

Wang Y, Subramanian M, Yurdagul A Jr., Barbosa-Lorenzi VC, Cai B, de Juan-Sanz J, Ryan TA, Nomura M, Maxfield FR, and Tabas I (2017). Mitochondrial Fission Promotes the Continued Clearance of Apoptotic Cells by Macrophages. Cell.

Waterham HR, Koster J, van Roermund CW, Mooyer PA, Wanders RJ, and Leonard JV (2007). A lethal defect of mitochondrial and peroxisomal fission. The New England journal of medicine 356, 1736–1741. [PubMed: 17460227]

Wieraszko A (1982). Changes in the hippocampal slices energy metabolism following stimulation and long-term potentiation of Schaffer collaterals-pyramidal cell synapses tested with the 2-deoxyglucose technique. Brain research 237, 449–457. [PubMed: 7083005]

Wu D, Bacaj T, Morishita W, Goswami D, Arendt KL, Xu W, Chen L, Malenka RC, and Sudhof TC (2017). Postsynaptic synaptotagmins mediate AMPA receptor exocytosis during LTP. Nature 544, 316–321. [PubMed: 28355182]

Xu S, Wang P, Zhang H, Gong G, Gutierrez Cortes N, Zhu W, Yoon Y, Tian R, and Wang W (2016). CaMKII induces permeability transition through Drp1 phosphorylation during chronic beta-AR stimulation. Nature communications 7, 13189.

Yoon G, Malam Z, Paton T, Marshall CR, Hyatt E, Ivakine Z, Scherer SW, Lee KS, Hawkins C, Cohn RD, et al. (2016). Lethal Disorder of Mitochondrial Fission Caused by Mutations in DNM1L. J Pediatr 171, 313–316 e311–312. [PubMed: 26825290]

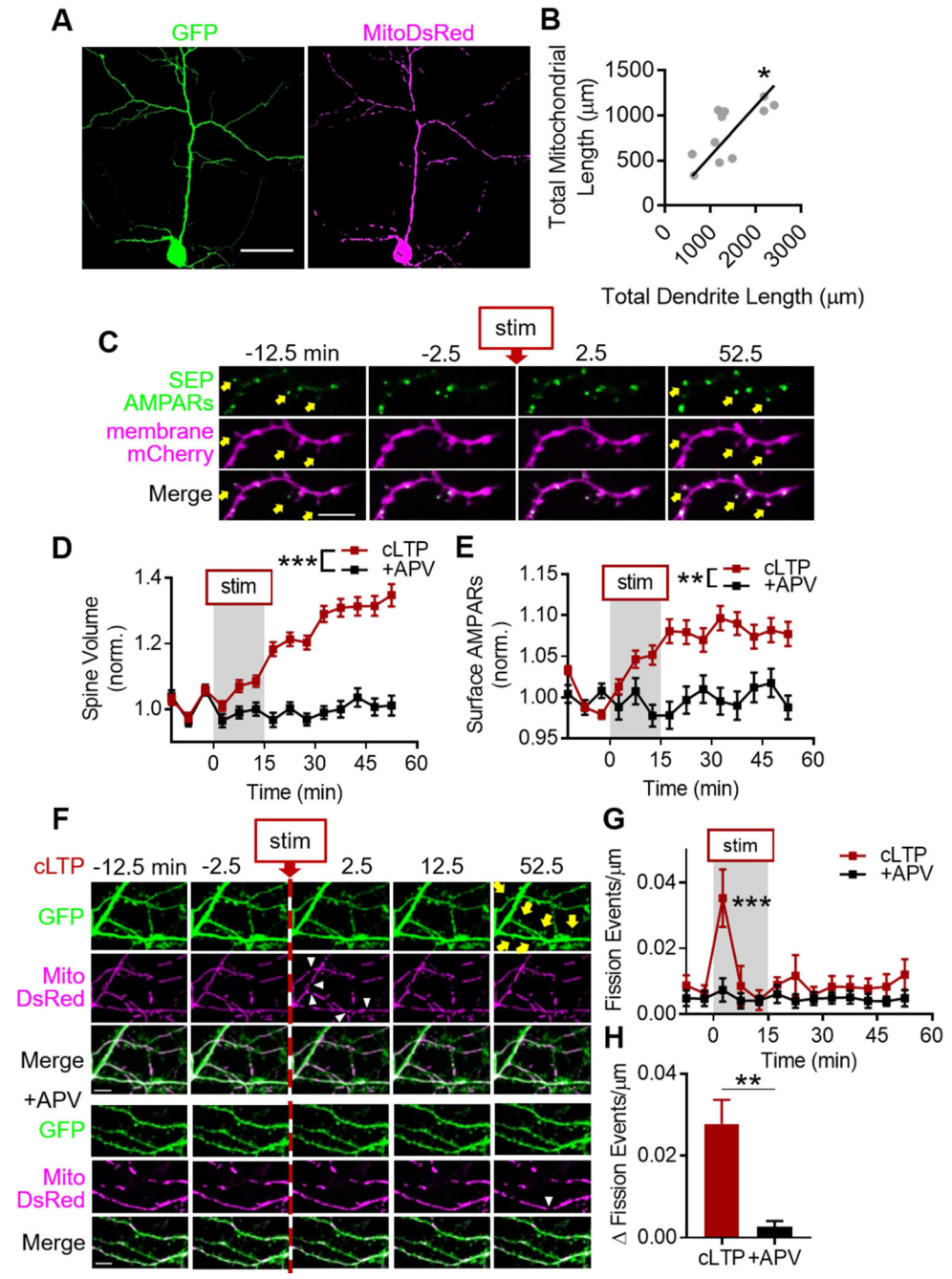

Figure 1. cLTP stimulation increases dendritic mitochondrial fission.

A) Representative images of pyramidal neuron expressing GFP and MitoDsRed. Scale bar: 50 μm. **B)** Total mitochondrial length and total dendrite length are correlated across many different cell sizes. Each gray circle represents one cell; black line is linear regression. **C-E)** cLTP stimulation increases dendritic spine volume and surface AMPARs. (C) Representative spines (yellow arrows). Scale bar: 5 μm. (D) Group spine volume and (E) surface AMPAR data. **F-H)** cLTP stimulation induces a rapid and large burst of dendritic mitochondrial fission, which is dependent on NMDAR activation. (F) *Top:* cLTP stimulation induces dendritic mitochondrial fission (white arrowheads) before spine growth (yellow arrows).

Bottom: APV treatment prevents fission burst. Scale bar: 5 μm. **G,H)** (G) Time-series and (H) change from baseline fission events per micron of dendrite. Data represented as mean ± SEM. *: $p<0.05$, **: $p<0.005$, ***: $p<0.0005$. Also see Figure S1.

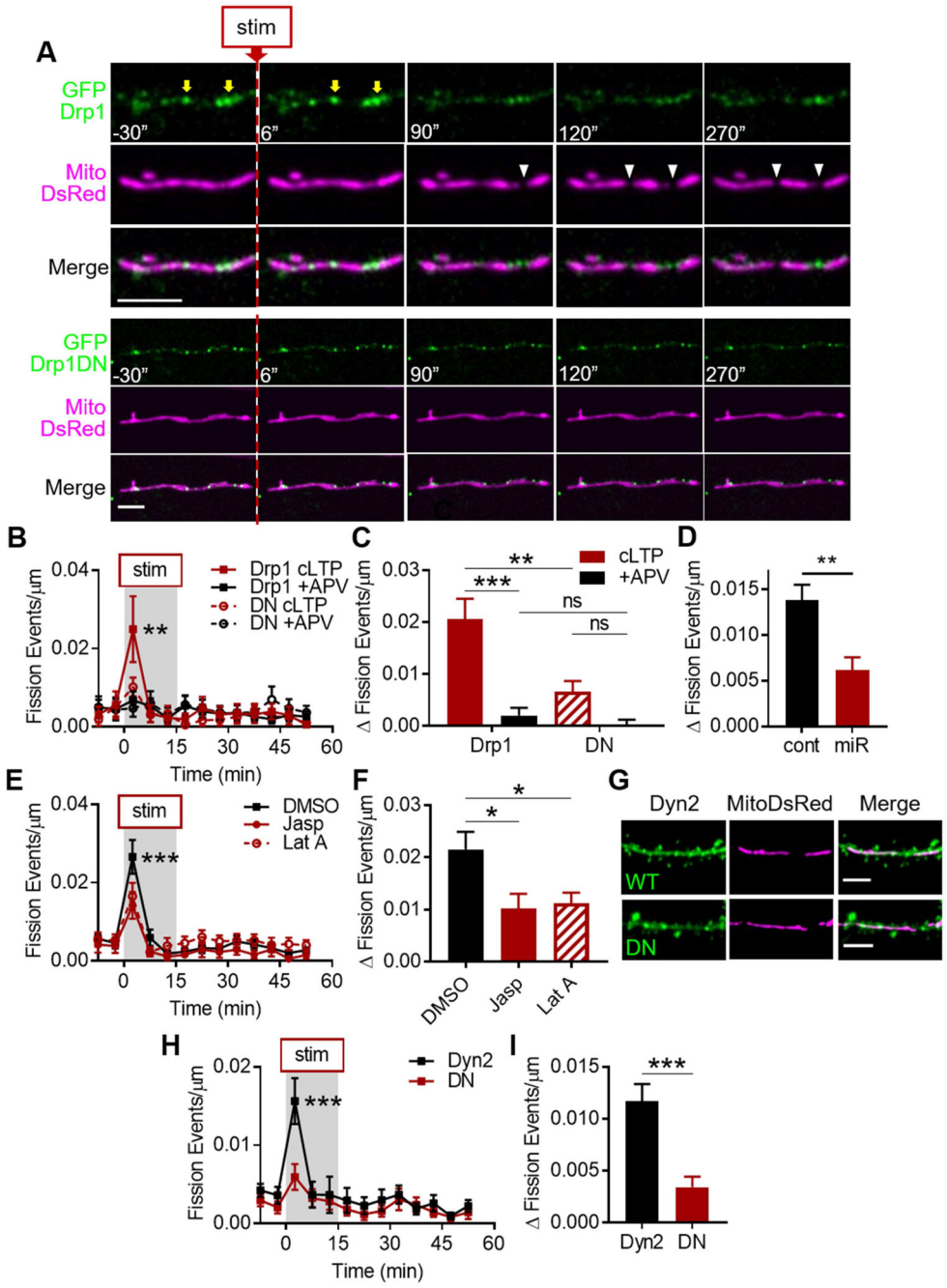

Figure 2. Molecular mechanisms underlying cLTP fission burst.

A) *Top:* Growing Drp1 puncta (yellow arrows) are found at sites of cLTP-evoked dendritic mitochondrial fission (white arrowheads) in cultured hippocampal neurons. *Bottom:* Drp1DN puncta on dendritic mitochondria are not associated with fission sites. Scale bar: 5 µm. Time in seconds. **B-D)** cLTP fission burst is Drp1-dependent. (B) Time-series and (C) change from baseline fission events per micron of dendrite in neurons expressing WT or DN Drp1. (D) Change from baseline in neurons expressing control or Drp1 miRNA. **E,F)** Actin dynamics contribute to cLTP fission burst. **G-I)** cLTP fission burst is Dyn2-dependent. (G) Representative images of dendrites, spines, and mitochondria in neurons expressing WT or

DN Dyn2. Data represented as mean ± SEM. ns: $p>0.05$, *: $p<0.05$, **: $p<0.005$, ***: $p<0.0005$. Also see Figures S2 and S3.

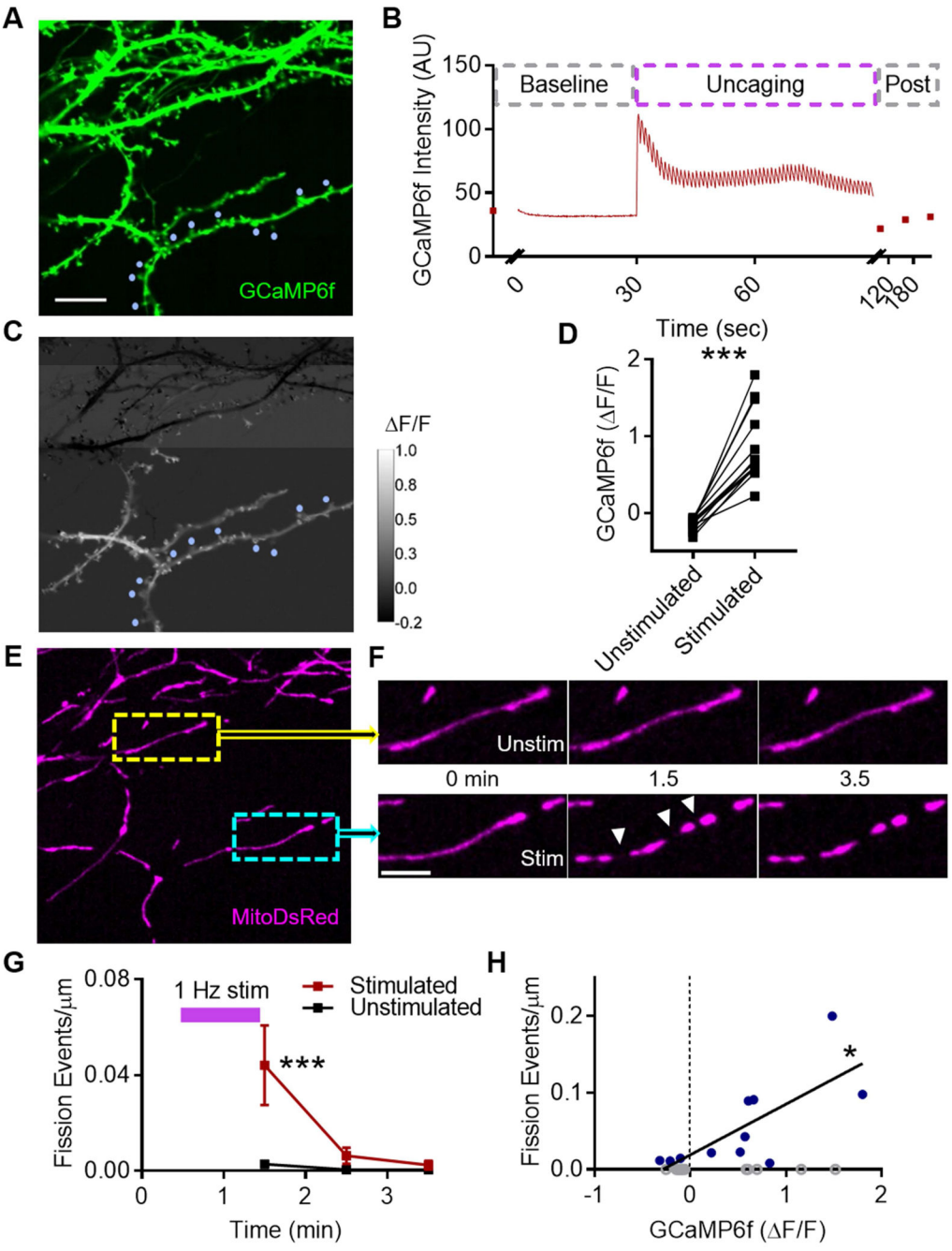

Figure 3. Cytosolic calcium elevation triggers mitochondrial fission.

A) Representative dendrites from cultured hippocampal neuron expressing GCaMP6f. Blue circles: stimulated spines. Scale bar: 10 µm. **B)** Representative time-series illustrating transient increase in dendrite GCaMP6f intensity following multi-spine glutamate photolysis. **C)** Color map illustrating spatial proximity of increase in GCaMP6f ΔF/F to stimulated spines. **D)** Glutamate photolysis only causes an increase in GCaMP6f ΔF/F in dendrites nearby stimulated spines, compared to unstimulated branches of the same cell. Each point represents an individual dendritic region. **E-H)** Mitochondrial fission selectively increases at sites of local cytosolic calcium elevation. (E) Representative image of

MitoDsRed within same neuron. Yellow inset: mitochondrion in GCaMP6f ΔF/F < 0 region. Cyan inset: mitochondria in GCaMP6f ΔF/F > 0. (F) Timeseries of insets in E. Fission events (white arrowheads). Scale bar: 5 μm. (G) Timecourse of mitochondrial fission events following photolysis train in stimulated and unstimulated region. Data represented as mean ± SEM. (H) Dendritic GCaMP6f ΔF/F is correlated with, and is predictive of, dendritic mitochondrial fission. Each point represents an individual dendritic region. Open gray circles: regions with zero fission events. Blue circles: regions with at least one fission event. *: $p<0.05$, ***: $p<0.0005$.

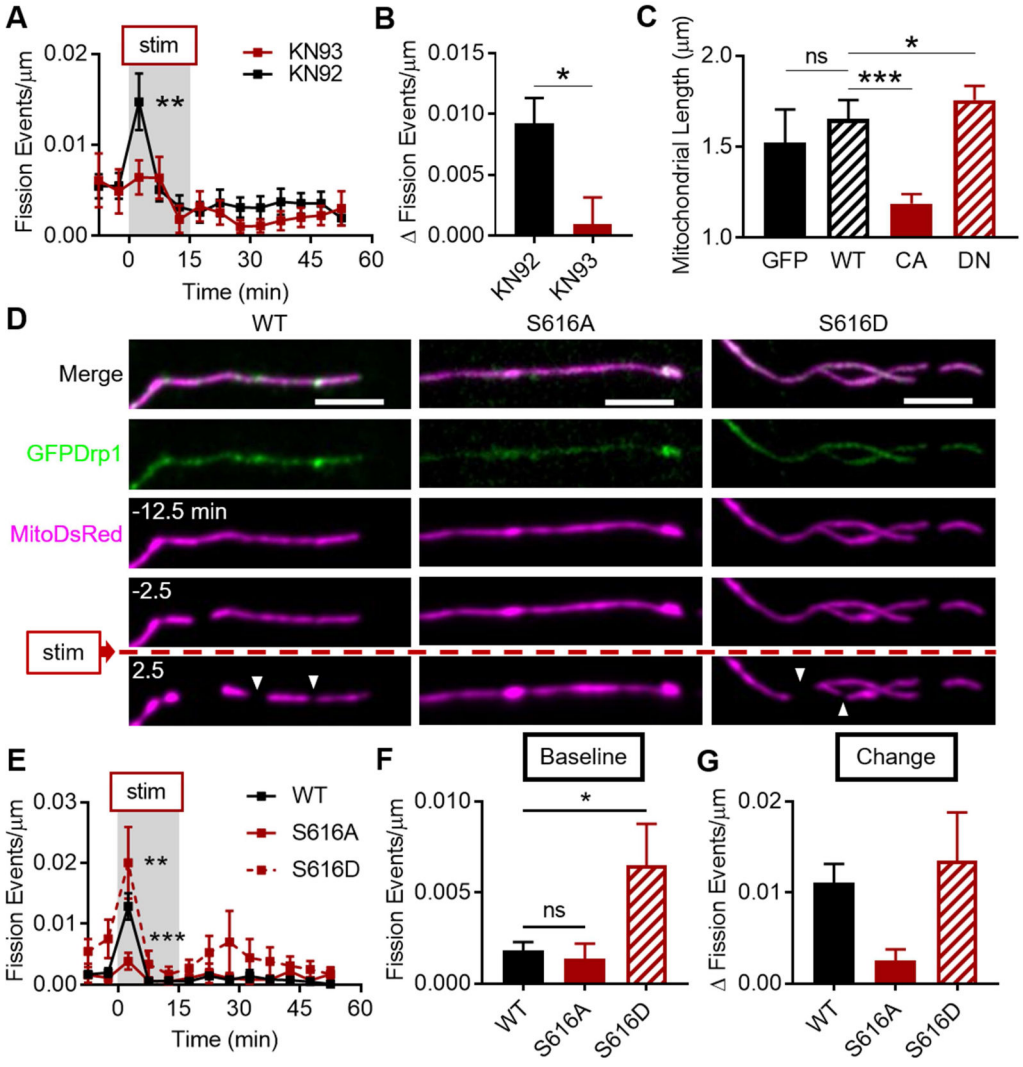

Figure 4. CaMKII and Drp1 phosphorylation are required for cLTP fission burst.

A-B) CaMKII activation is required for cLTP fission burst. Data represented as mean ± SEM. **C)** CaMKII activity level controls baseline mitochondrial length. Data represented as median ± 95% CI. **D-G)** Drp1 Ser616 phosphorylation is required for the cLTP fission burst. (D) Representative timeseries of cLTP fission burst (white arrowheads) in neurons expressing MitoDsRed and GFP-tagged WT, S616A (phospho-null), or S616D (phospho-mimetic) Drp1 variants. Scale bar: 5 µm. (E) Fission burst is prevented by Drp1 S616A. (F) Baseline fission rate is enhanced by S616D. (G) Fission change from baseline among the three groups. Data represented as mean ± SEM. ns: $p>0.05$, *: $p<0.05$, **: $p<0.005$, ***: $p<0.0005$. Also see Figure S4.

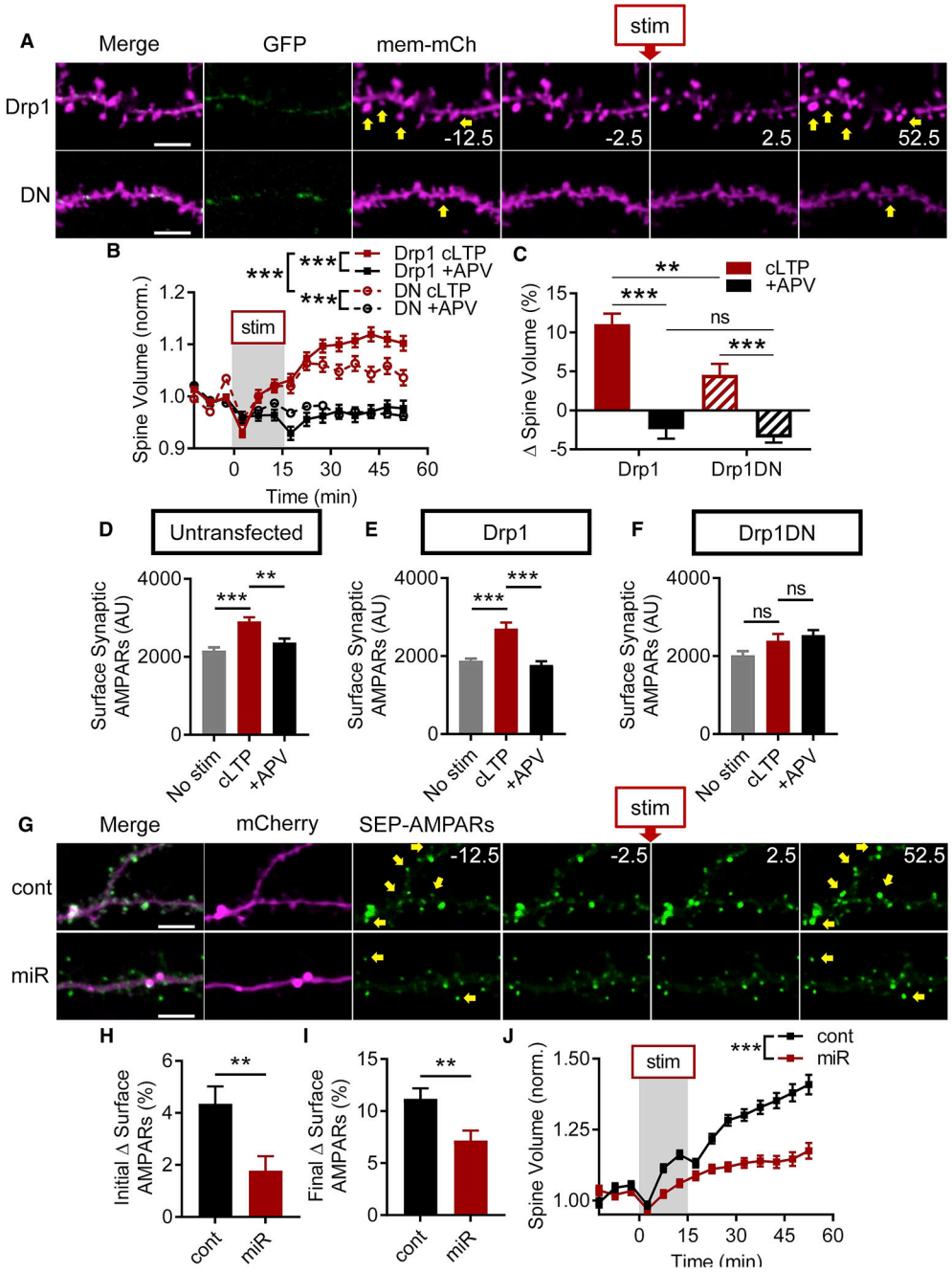

Figure 5. Dendritic mitochondrial fission is required for structural LTP.

A-C) Dendritic spine growth after cLTP stimulation is impaired in neurons expressing GFPDrp1DN. (A) Representative dendrites illustrating dendritic spine growth after stimulation (yellow arrows). Scale bar: 5 μm. Time in minutes. (B) Spine volume timeseries and (C) final percent change in spine volume are impaired by Drp1DN. **D-I)** Mitochondrial fission is required for increasing surface synaptic AMPARs during LTP. (D-F) GFPDrp1DN prevents increase in surface synaptic AMPARs - immunocytochemistry. (G-I) Drp1 miRNA (miR) prevents increase in surface AMPARs – SEP-AMPARs. (G) Representative dendrites and timeseries from neurons expressing control (cont) or Drp1 miRNA. Scale bar: 5 μm.

Time in minutes. (H) Initial and (I) final change in surface AMPARs are impaired. **J)** Drp1 miR prevents dendritic spine growth after cLTP stimulation. Data represented as mean ± SEM. ns: $p>0.05$, **: $p<0.005$, ***: $p<0.0005$. Also see Figure S5.

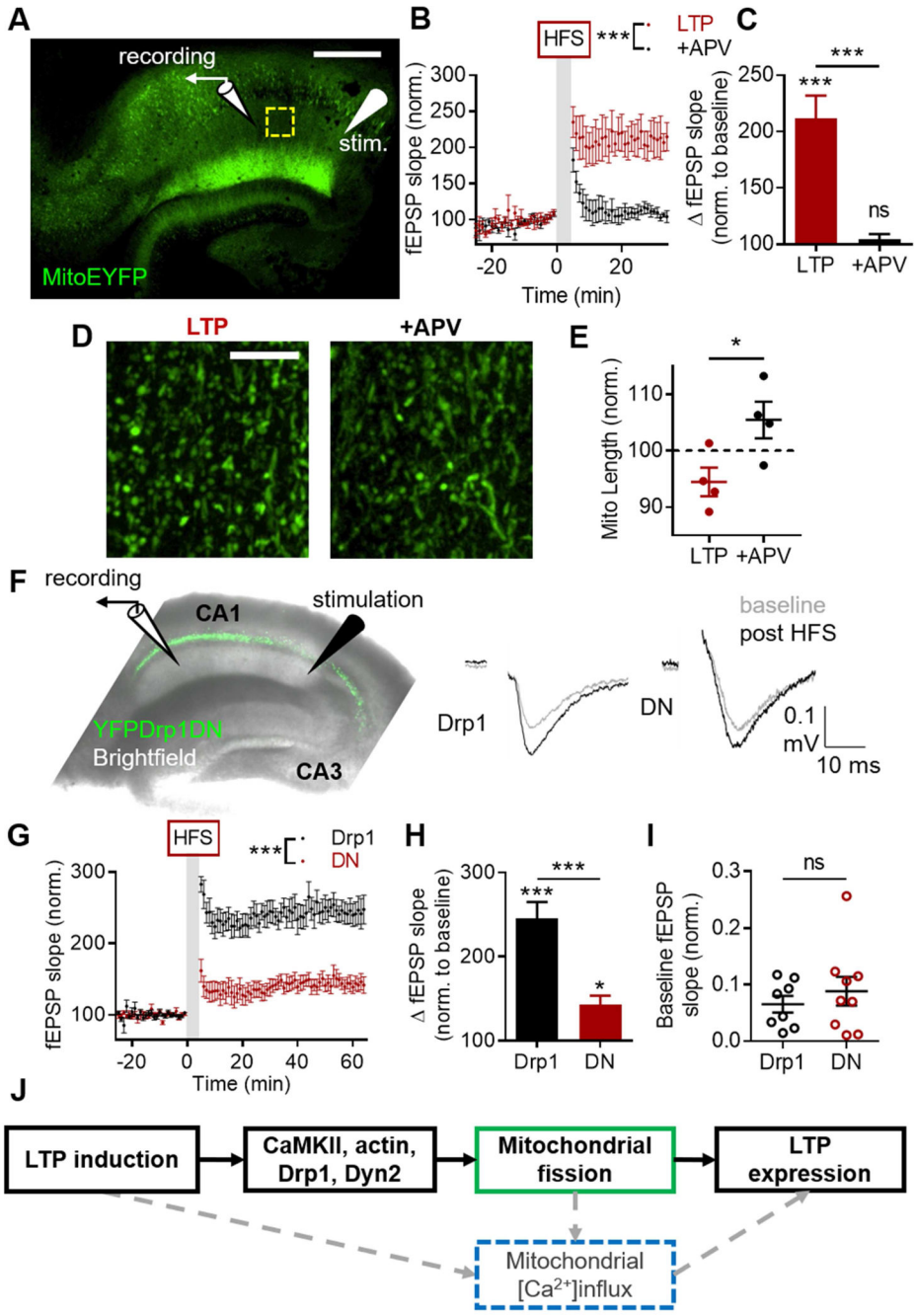

Figure 6. Dendritic mitochondrial fission is required for electrophysiological LTP.

A-E) HFS of Schaffer collaterals produces shorter mitochondria in CA1 stratum radiatum in acute hippocampal slices. (A) Representative image of cleared acute hippocampal slice from MitoEYFP transgenic mouse with schematic of stimulation paradigm. Yellow box: example imaging region. Scale bar: 500 μm. (B-C) HFS produces robust NMDAR-dependent LTP. (D) Example of CA1 mitochondria in slices after HFS in normal ACSF (*left*) and +APV (*right*). Scale bar: 10 μm. (E) HFS produces shorter mitochondria in CA1 dependent on NMDAR activation. **F-H)** Preventing dendritic mitochondrial fission with DN Drp1 suppresses HFS-LTP in hippocampal slices. (F) *Left:* Diagram of electrophysiology

experiment design in hippocampal slice infected with YFPDrp1DN. *Right:* Example traces illustrating LTP of CA1 fEPSPs in slices expressing Drp1 or Drp1DN. (G) Group data showing the effect of DN Drp1 on HFS of CA1 fEPSPs over time. (H) Drp1DN impairs HFS LTP of Schaffer collateral-CA1 synapses. (I) Basal AMPAR synaptic transmission is not impacted by infecting slices with Drp1DN. **J)** Model. Solid boxes, black lines: findings of the current study. Dashed boxes, gray lines: proposed mechanisms. Data represented as mean ± SEM. ns: $p>0.05$, *: $p<0.05$, ***: $p<0.0005$. Also see Figure S6.

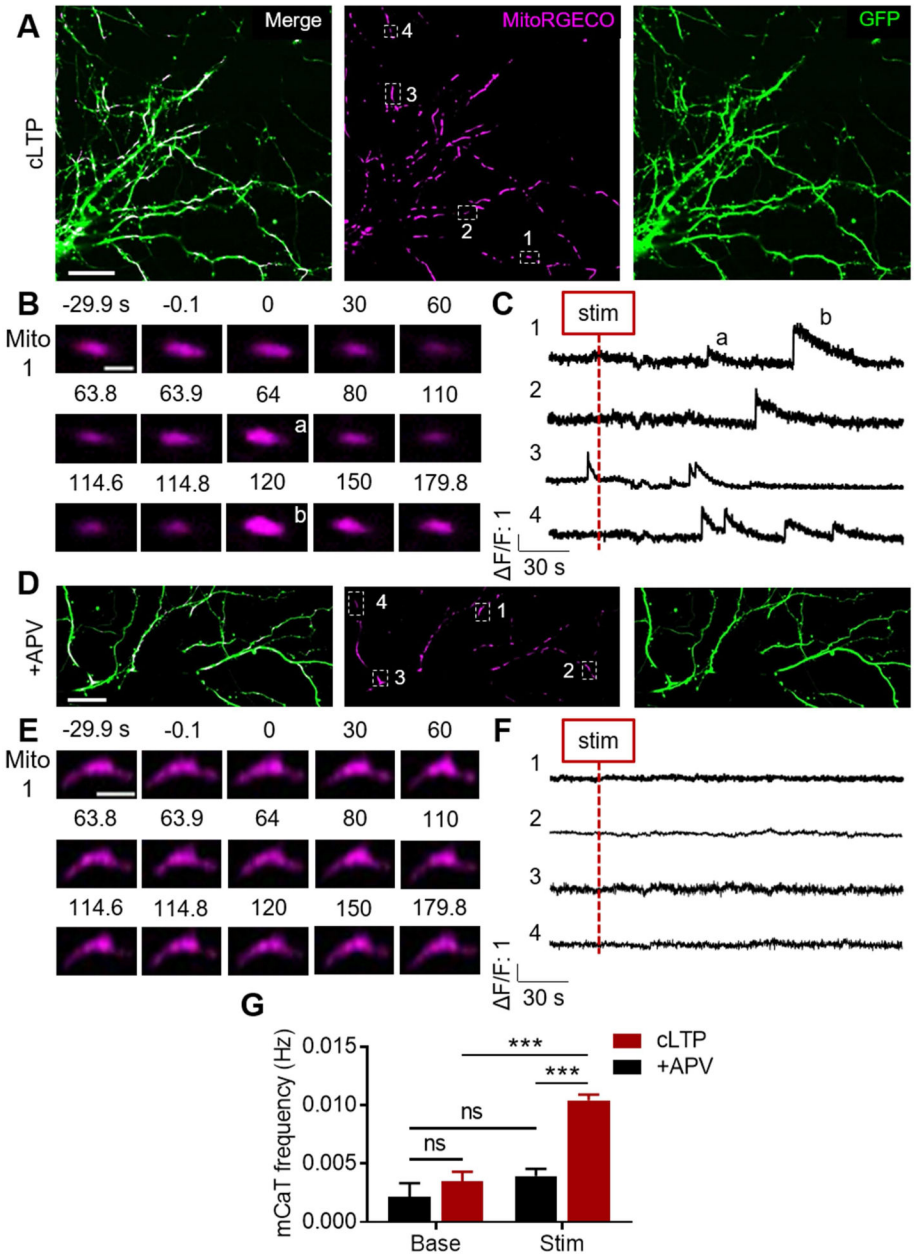

Figure 7. cLTP stimulation increases the frequency of mitochondrial calcium transients (mCaTs).

A) Representative images of cLTP-stimulated cultured hippocampal neuron expressing GFP and MitoRGECO. Scale bar: 25 μm. **B)** Representative timeseries of single dendritic mitochondrion depicting two cLTP-evoked mCaTs. Scale bar: 2 μm. **C)** Representative ΔF/F traces from dendritic mitochondria depicting cLTP-evoked mCaTs. **D)** Representative image of +APV-stimulated cultured hippocampal neuron. Scale bar: 25 μm. **E)** Representative timeseries (Scale bar: 4 μm) and **F)** ΔF/F traces of individual dendritic mitochondria showing no mCaTs following stimulation. **G)** cLTP stimulation causes an NMDAR-dependent increase in dendritic mCaT frequency. Data represented as mean ± SEM. ns: $p>0.05$, ***: $p<0.0005$. Also see Figure S7.

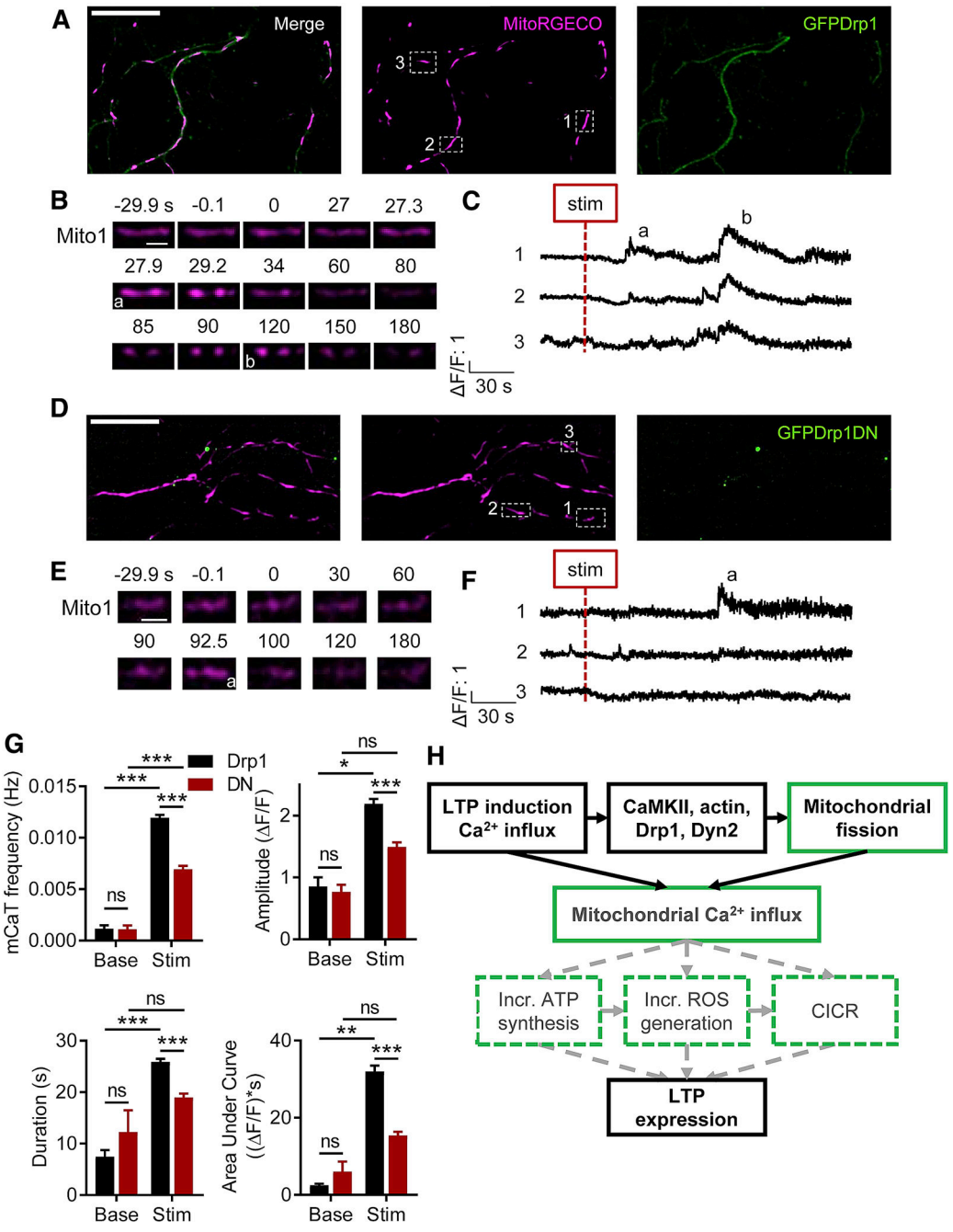

Figure 8. cLTP-evoked dendritic mCaTs require mitochondrial fission.

A,D) Representative image of cLTP-stimulated cultured hippocampal neuron expressing MitoRGECO and (A) GFP Drp1 or (D) Drp1DN. Scale bar: 25 μm. **B,E)** Representative timeseries of single dendritic mitochondrion depicting cLTP-evoked mCaTs in (B) GFPDrp1 or (E) Drp1DN neurons. Scale bar: 2.5 μm. **C,F)** Representative ΔF/F traces from dendritic mitochondria depicting cLTP-evoked mCaTs in (C) GFPDrp1 or (F) Drp1DN neurons. **G)** cLTP-evoked mCaT frequency, amplitude, duration, and integrated area require dendritic mitochondrial fission. **H)** Potential mechanisms by which dendritic mitochondrial fission and mCaTs may regulate LTP. Solid boxes, black lines: findings of the current study. Dashed

boxes, gray lines: proposed mechanisms. Data represented as mean ± SEM. ns: $p>0.05$, *: $p<0.05$, **: $p<0.005$, ***: $p<0.0005$.

KEY RESOURCES TABLE

REAGENT or RESOURCE	SOURCE	IDENTIFIER
Antibodies		
Rabbit anti-Drp1 (D6C7)	Cell Signaling Technologies	Cat. #8570, RRID:AB_10950498
Rabbit anti-Homer1	Synaptic Systems	Cat. #160003, RRID:AB_887730
Mouse anti-GluA2	Millipore	Cat. #Mab397, RRID:AB_2113875
Donkey anti-Rabbit-Alexa647	Jackson Immuno Research	Cat. #711-605-152, RRID:AB_2492288
Goat anti-Mouse-Atto565	Hypermol	Cat. #2117, RRID:AB_2736914
Bacterial and Virus Strains		
AAV2-MitoDsRed	This paper	N/A
AAV1-CAG-GCaMP6f.WPRE.SV40	Penn Vector Core	Cat. #P3081
AAV2-Cre-GFP	UNC Vector Core	N/A
AAV2-DIO-Drp1(WT)-EYFP	(Chandra et al., 2017)	N/A
AAV2-DIO-Drp1(K38A)-EYFP	This paper	N/A
Chemicals, Peptides, and Recombinant Proteins		
DL-2-Amino-5-phosphonopentanoic acid (APV)	Sigma	Cat. #A5282
Picrotoxin	Sigma	Cat. #P1675
Tetrodotoxin	Millipore	Cat. #554412
Strychnine	Sigma	Cat. #S0532
Jasplakinolide	Invitrogen	Cat. #J7473
Latrunculin A	Sigma	Cat. #L5163
KN-93	Millipore	Cat. #422708
KN-92	Millipore	Cat. #422709
Mdivi-1	Sigma	Cat. #M0199
CGP52432	Tocris	Cat. #1246
MNI-caged-L-glutamate	Tocris	Cat. #1490
Critical Commercial Assays		
KAPA HiFi DNA Polymerase	Kapa Biosystems	Cat. #KK2101
Q5 Site-Directed Mutagenesis Kit	New England Biolabs	Cat. #E0554

REAGENT or RESOURCE	SOURCE	IDENTIFIER
Gel DNA Recovery Kit	Zymo Research	Cat. #D4007
AAVpro Purification Kit	TaKara Bio	Cat. #6666
Experimental Models: Organisms/Strains		
Rat: Sprague Dawley (Strain code 400)	Harlan/Envigo	N/A
Mouse: CaMKII-MitoEYFP	(Chandrasekaran et al., 2006).	The Jackson Laboratory Cat. #006618
Mouse: WT C57BL/6J	The Jackson Laboratory	Cat. #000664
Oligonucleotides		
KD_FW: GCCGTCGATCGTTTAAACGGAG	This paper	N/A
KD_REV: GGTTTTAAAGCCTGCTTTTTTGTACAAACT	This paper	N/A
mCh_FW: GCAGGCTTTAAAACCATGGTGAGCAAGGGCGAGGA	This paper	N/A
mCh_REV: TAAACGATCGACGGCTACTTGTACAGCTCGTCCATGCC	This paper	N/A
Drp1-S616A_FW: TATGCCAGCAGCTCCACAAAAAGGC	This paper	N/A
Drp1-S616A_REV: ATTGGAATTGGTTTTGATTTTTC	This paper	N/A
Drp1-S616D_FW: TATGCCAGCAGATCCACAAAAAGGC	This paper	N/A
Drp1-S616D_REV: ATTGGAATTGGTTTTGATTTTTC	This paper	N/A
Drp1_FW: CTTCCCAGAGGGACTGGTGTG	This paper	N/A
Drp1_REV: ACTAATTCACTCTGAAGAGTA	This paper	N/A
Recombinant DNA		
EGFP-Drp1(WT)	Gift from H.N. Higgs, Dartmouth	N/A
MitoDsRed	Gift from H.N. Higgs, Dartmouth	N/A
MitoRGECO	Gift from H.N. Higgs, Dartmouth	N/A
EGFP-Drp1(K38A)	Gift from S. Strack, U. Iowa	N/A
EGFP-Dyn2(WT)	Gift from P. Welling, U. Maryland via P. De Camilli, Yale	N/A
EGFP-Dyn2(K44A)	Gift from P. Welling, U. Maryland via P. De Camilli, Yale	N/A
SEP-GluA1	Gift from R. Huganir, Johns Hopkins	N/A
SEP-GluA2	Gift from R. Huganir, Johns Hopkins	N/A
mCherry::Drp1-miRNA	This paper	N/A
mCherry::Drp1-controlRNA	This paper	N/A
EGFP-Drp1(S616A)	This paper	N/A

REAGENT or RESOURCE	SOURCE	IDENTIFIER
EGFP-Drp1(S616D)	This paper	N/A
Software and Algorithms		
Prism 7.0	GraphPad	https://www.graphpad.com/scientific-software/prism/
ImageJ FIJI	National Institutes of Health	https://fiji.sc/
MetaMorph	Molecular Devices	https://www.moleculardevices.com/products/cellular-imaging-systems/acquisition-and-analysis-software/metamorph-microscopy
Mytoe	(Lihavainen et al., 2012)	http://www.cs.tut.fi/~sanchesr/tool_Mytoe/MyToe.html
MATLAB	MathWorks	https://www.mathworks.com/products/matlab.html
Clampfit 10.7	Molecular Devices	https://www.moleculardevices.com/products/axon-patch-clamp-system/acquisition-and-analysis-software/pclamp-software-suite